JYVÄSKYLÄ STUDIES IN BIOLOGICAL AND ENVIRONMENTAL SCIENCE

272

Mikko Ylilauri

Effect of Ligand-Binding on Protein Function

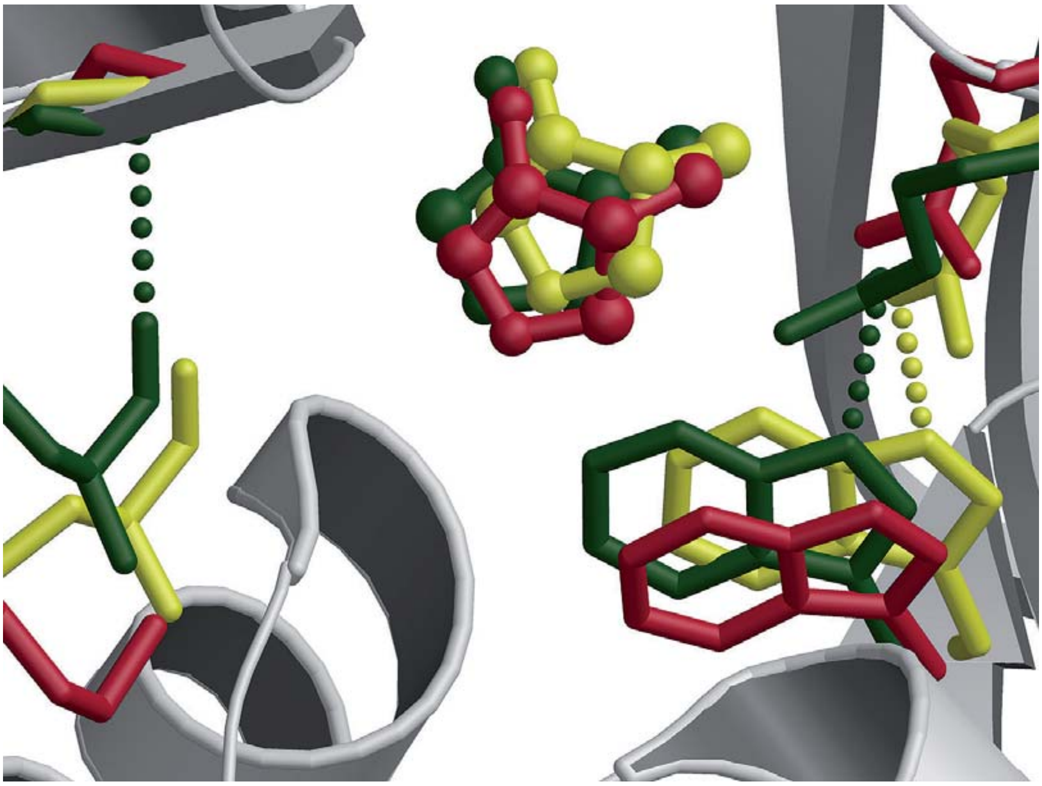

JYVÄSKYLÄN YLIOPISTO

JYVÄSKYLÄ STUDIES IN BIOLOGICAL AND ENVIRONMENTAL SCIENCE 272

Mikko Ylilauri

Effect of Ligand-Binding on Protein Function

Esitetään Jyväskylän yliopiston matemaattis-luonnontieteellisen tiedekunnan suostumuksella
julkisesti tarkastettavaksi yliopiston Ylistönrinteellä, salissa YAA303
tammikuun 24. päivänä 2014 kello 12.

Academic dissertation to be publicly discussed, by permission of
the Faculty of Mathematics and Science of the University of Jyväskylä,
in Ylistönrinne, hall YAA303, on January 24, 2014 at 12 o'clock noon.

UNIVERSITY OF JYVÄSKYLÄ

JYVÄSKYLÄ 2014

Effect of Ligand-Binding on Protein Function

JYVÄSKYLÄ STUDIES IN BIOLOGICAL AND ENVIRONMENTAL SCIENCE 272

Mikko Ylilauri

Effect of Ligand-Binding on Protein Function

UNIVERSITY OF JYVÄSKYLÄ

JYVÄSKYLÄ 2014

Editors
Varpu Marjomäki
Department of Biological and Environmental Science, University of Jyväskylä
Pekka Olsbo, Ville Korkiakangas
Publishing Unit, University Library of Jyväskylä

Jyväskylä Studies in Biological and Environmental Science
Editorial Board

Jari Haimi, Anssi Lensu, Timo Marjomäki, Varpu Marjomäki
Department of Biological and Environmental Science, University of Jyväskylä

Cover picture by Mikko Ylilauri.

URN:ISBN:978-951-39-5583-0
ISBN 978-951-39-5583-0 (PDF)

ISBN 978-951-39-5582-3 (nid.)
ISSN 1456-9701

Copyright © 2014, by University of Jyväskylä

Jyväskylä University Printing House, Jyväskylä 2014

Tuomakselle

ABSTRACT

Ylilauri, Mikko
Effect of ligand-binding on protein function
Jyväskylä: University of Jyväskylä, 2014, 61 p.
(Jyväskylä Studies in Biological and Environmental Science
ISSN 1456-9701; 272)
ISBN 978-951-39-5582-3 (nid.)
ISBN 978-951-39-5583-0 (PDF)
Yhteenveto: Ligandin sitoutumisen vaikutus proteiinin toimintaan
Diss.

Ligand-binding in a specific manner is vital to all cellular actions and can have a major effect on the activity and conformation of proteins. In addition to experimental techniques, computational methods, such as molecular dynamics (MD) simulations, have become an integral part in studies related to protein-ligand interactions. The computational approach introduces a dynamic view of molecular interactions, and enables detailed structure-function studies. In addition, it may facilitate the estimation of binding affinities and help in identifying ligand-binding sites in proteins. In this thesis three pharmacologically important protein targets were studied with both computational and experimental methods: 1) ionotropic glutamate receptors (iGluRs), 2) filamin A (FLNa), and 3) T-cell protein tyrosine phosphatase (TCPTP). iGluRs mediate synaptic transmission in the nervous system and are linked to many neurological disorders. Partial agonism of the ligand binding domains (LBD) for these receptors was studied with MD simulations and the molecular mechanics generalised Born surface area (MM-GBSA) method. A previously unobserved intermediate closure stage for the GluN1 receptor subtype was identified, and new information about the closure mechanism was obtained. FLNa is an actin cross-linking protein linked to many cellular functions via its numerous binding partners. MM-GBSA calculations of binding free energy were shown to correlate well with the experimental data. Thus, ligands could be ranked based on their binding affinity, suggesting that also the rational design of FLNa-binding peptide mimetics would be conceivable. TCPTP is a ubiquitously expressed non-transmembrane phosphatase that negatively regulates many cancer-related kinases. TCPTP is normally auto-inhibited, but several agonist molecules are known to activate it. Here, a putative binding site for TCPTP activators was identified and important structural determinants for novel activators were recognised. As TCPTP is not down-regulated in cancer cells, it is a promising target for tumor suppression.

Keywords: Binding free energy; filamin; ionotropic glutamate receptor; molecular dynamics; T-cell protein tyrosine phosphatase.

Mikko Ylilauri, University of Jyväskylä, Department of Biological and Environmental Science, P.O. Box 35, FI-40014 University of Jyväskylä, Finland

Author's address
Mikko Ylilauri
Department of Biological and Environmental Science
P.O. Box 35
FI-40014 University of Jyväskylä
Finland
mikko.ylilauri@jyu.fi

Supervisor
Adjunct Professor Olli Pentikäinen
Department of Biological and Environmental Science
P.O. Box 35
FI-40014 University of Jyväskylä
Finland

Reviewers
Associate Professor Geoffrey Swanson
Molecular Pharmacology and Biological Chemistry
Northwestern University
Feinberg School of Medicine
303 E Chicago Ave
Chicago, USA 60611

Adjunct Professor Mikael Peräkylä
Department of Pharmacy
University of Eastern Finland
P.O. Box 1627
FI-70211 Kuopio
Finland

Opponent
Dr. Philip Biggin
Department of Biochemistry
University of Oxford
South Parks Road
Oxford OX1 3QU
United Kingdom

CONTENTS

ABSTRACT
CONTENTS
LIST OF ORIGINAL PUBLICATIONS
RESPONSIBILITIES OF MIKKO YLILAURI IN THE THESIS ARTICLES
ABBREVIATIONS

1 INTRODUCTION 11

2 REVIEW OF THE LITERATURE 13
  2.1 Glutamate receptors 13
    2.1.1 Ionotropic glutamate receptors 13
    2.1.2 Ligand-binding domain structure and activation 15
    2.1.3 Partial agonism of GluN1 16
  2.2 Filamin A 17
    2.2.1 FLNa interaction with ligand peptides 19
    2.2.2 FLNa domains with a conserved CD-face 20
  2.3 T-cell protein tyrosine phosphatase 20

3 AIMS OF THE STUDY 24

4 METHODS 25
  4.1 Databases 25
  4.2 Homology modeling 25
  4.3 Ligand molecules 25
  4.4 Structure comparison and ligand positioning 26
  4.5 Molecular dynamics simulations 26
    4.5.1 Constraint-free molecular dynamics simulations 27
    4.5.2 Steered molecular dynamics simulations 28
  4.6 MM-GBSA 28
  4.7 Experimental methods 30
    4.7.1 Isothermal titration calorimetry 30
    4.7.2 Differential scanning fluorimetry 30
    4.7.3 Other experimental methods utilised 31
  4.8 Visualisation 31

5 RESULTS 32
  5.1 Ionotropic glutamate receptors (I, II) 32
    5.1.1 Interdomain H-bond efficiently indicates cleft closure (I) 32
    5.1.2 Full agonists maintain the LBD closed in MD simulations (I) 33
    5.1.3 Partial agonists destabilise closed-cleft iGluRs (I) 33
    5.1.4 MD simulations reveal an intermediate closure stage for GluN1 (I, II) 33
    5.1.5 SMD simulations mimic forces affecting the GluN1-LBD closure (II) 34
    5.1.6 Closure mechanism of GluN1-LBD (II) 34

5.1.7 Energetic basis of the GluN1-LBD closure (II) 35
5.2 Filamin A interaction with peptide-ligands (III)......................................35
5.2.1 Peptide-ligand-bound Filamin A MM-GBSA calculations compared to experimental data...36
5.2.2 SMD simulations of FLNa21-peptide complexes 36
5.2.3 FLN-related biological problems studied with MM-GBSA 37
5.3 T-cell protein tyrosine phosphatase activation by small molecules (IV)...37

6 DISCUSSION 40
6.1 Ionotropic glutamate receptors 40
6.1.1 IHB disruption enables categorisation of ligands as full or partial agonists 40
6.1.2 The mechanism of intermediate closure of GluN1-LBD.............41
6.2 Filamin A interaction with peptide-ligands 42
6.2.1 MM-GBSA is able to rank ligand-peptides according to their binding affinities 42
6.2.2 SMD confirms the critical interactions between FLNa and bound peptide 43
6.3 TCPTP activation by small molecules 43

7 CONCLUSIONS...45

Acknowledgements
YHTEENVETO (RÉSUMÉ IN FINNISH)
REFERENCES

LIST OF ORIGINAL PUBLICATIONS

The thesis is based on the following original articles, which will be referred to in the text by their Roman numerals.

I Postila P.A., Ylilauri M. & Pentikäinen O.T. 2011. Full and partial agonism of ionotropic glutamate receptors indicated by molecular dynamics simulations. *Journal of Chemical Information and Modeling* 51: 1037–1047.

II Ylilauri M. & Pentikäinen O.T. 2012. Structural mechanism of *N*-methyl-D-aspartate receptor type 1 partial agonism. *PLoS One* 7 (10): e47604.

III Ylilauri M. & Pentikäinen O.T. 2013. MMGBSA as a tool to understand the binding affinities of filamin-peptide interactions. *Journal of Chemical Information and Modeling* 53: 2626-2633

IV Ylilauri M., Mattila E., Nurminen E.M., Käpylä J., Niinivehmas S.P., Määttä J.A., Pentikäinen U., Ivaska J. & Pentikäinen O.T. 2013. Molecular mechanism of T-cell protein tyrosine phosphatase (TCPTP) activation by mitoxantrone. *Biochimica et Biophysica Acta* 1834: 1988-1997

RESPONSIBILITIES OF MIKKO YLILAURI IN THE THESIS ARTICLES

Article I	I completed the MD simulations and RMSD calculations related to GluN1. I made the cleft-closure and interdomain hydrogen bond angle measurements for all protein-ligand complexes, and prepared the figures related to these experiments. I wrote the article together with Pekka Postila and Olli Pentikäinen.
Article II	I designed the study together with Olli Pentikäinen, and completed all of the simulations. I wrote the article and made the figures.
Article III	I designed the study together with Olli Pentikäinen, and completed all of the simulations. I wrote the article and made the figures.
Article IV	I did all the computational studies described in the article. I participated in the protein expression and purification, and I conducted all of the DSF experiments described in the article and most of the ITC measurements with mitoxantrone. I wrote the article together with other authors, and prepared the majority of the figures.

ABBREVIATIONS

α1-cyt	cytoplasmic tail of α1-integrin
ACBC	1-aminocyclobutane-1-carboxylic acid
ACPC	1-aminocyclopropane-1-carboxylic acid
AMPA	(S)-2-amino3-(3-hydroxy-5-methyl-4-isoxazolyl) propionic acid
ATD	amino-terminal domain
DCS	D-cycloserine
DSF	differential scanning fluorimetry
EGFR	epidermal growth factor receptor
FLNa	filamin A
GluA1-4	AMPA receptor subunits
GluK1-5	kainate receptor subunits
GluN1-3	NMDA receptor subunits
GP	generalised Born model for continuum solvent
GPIbα	glycoprotein Ibα
H-bond	hydrogen bond
iGluR	ionotropic glutamate receptor
IHB	interdomain hydrogen bond
ITC	isothermal titration calorimetry
LBD	ligand-binding domain
MD	molecular dynamics
mGluR	metabotropic glutamate receptor
MM-GBSA	molecular mechanics generalised Born surface area
NMDA	*N*-methyl-D-aspartic acid
PDB	Protein Data Bank
PB	Poisson-Boltzmann model for continuum solvent
PTK	protein tyrosine kinase
PTP	protein tyrosine phosphatase
R^2	coefficient of determination
RTK	receptor tyrosine kinase
SMD	steered molecular dynamics
TCPTP	T-cell protein tyrosine phosphatase
TC33	constitutively active 33 kDa form of TCPTP
TC37	constitutively active 37 kDa form of TCPTP
TC45	45 kDa form of TCPTP
TC48	48 kDa form of TCPTP
T_m	melting temperature
TMD	transmembrane domain

1 INTRODUCTION

Proteins are the most abundant and diverse macromolecules in living cells. They are involved in a tremendous number of processes, such as signal transduction as receptor proteins, metabolism as enzymes, cell shape maintenance as structural proteins, and homeostasis maintaining as hormones. In addition to their versatile roles, proteins also cover a wide range of different structures and sizes. However, eventually every protein is built based on the same set of 20 amino acids joined together in different combinations.

The functions of proteins are strongly dependent on interactions with ligands. In contrast to substrates, which are modified by enzymes, the binding of a ligand into a protein is typically reversible. However, this transient interaction between proteins and ligands is essential for all life, and the biological areas they affect range from neuronal signalling to hormone activity and cell division. In many cases, proteins have a significant effect on the activity and conformation of the protein. The specific binding is the key to protein-ligand interaction: only molecules with size, shape, and charge complementary to the binding site are able to attach firmly enough to be distinguished from other molecules. This specific recognition is vital for normal protein function and also forms the basis for novel drug development.

During the past years, the rapid development of computer processors has accelerated research in the biological sciences to a new level. Nowadays, both experimental and computational methods can be successfully combined in the structure-function studies of proteins in complex with their ligand molecules. This combinatory utilisation of both the *in silico* and *in vitro* approaches is beneficial for our knowledge of the various protein-ligand interactions. For example, by gaining atom-level information of the ligand-binding event and the structural features affecting it, rational drug design can be significantly advanced.

While experimentally obtained structures are still desirable and substantial for the detailed study of proteins, homology modelling, and force field based methods, such as molecular dynamics simulations (MD) can offer benefits at all stages of study. In the absence of 3D-structures, a homology model based on earlier solved structures of similar proteins may provide the first reasonable view of the protein structure. Furthermore, computational ligand docking can help to identify the putative binding modes and interactions with the protein. Even if crystal structures for the proteins of interest exist, they are intrinsically static in nature and do not show the dynamic fluctuation of the protein. MD simulations, on the other hand, take into account the dynamics of the interactions. Consequently, they can estimate the ligand-binding stability as well as the possible changes in conformations of both binding partners. In addition, the free energy calculations based on MD simulation trajectories may provide further information, for example, a closer look into the affinities of different ligands. Naturally there are some limitations regarding the MD simulations that must be kept in mind. As the proteins in this method are taken out of their natural cellular context, the possible interaction partner proteins are missing from the simulations. In addition, force fields utilized in MD are based on many approximations that may affect the results. It may also be hard to validate the MD results for example to justify if the simulation has proceeded in a reasonably direction.

In this doctoral thesis various pharmacologically interesting protein-ligand interactions were studied to shed light on these specific events, and also to evaluate the usefulness of the computational methods in the study of these interactions. MD simulations and other sophisticated computational methods were utilised to study 1) the full and partial agonist binding to ionotropic glutamate receptors, 2) filamin A's interaction with ligand-peptides, and 3) T-cell protein tyrosine phosphatase (TCPTP) activation. In the case of TCPTP, experimental methods were also applied to complement the computational approach.

2 REVIEW OF THE LITERATURE

2.1 Glutamate receptors

Glutamate receptors mediate excitatory synaptic transmission in the mammalian nervous system. They are essential for brain function because glutamate is the most prominent excitatory neurotransmitter in the central nervous system. The mammalian glutamate receptors are divided into two distinct sub-families based on their activation mechanism: metabotropic (mGluRs) and ionotropic glutamate receptors (iGluRs). While both receptor types are activated via binding of a neurotransmitter to the extracellular ligand-binding site, the mechanisms of action differ: iGluRs have an ion channel in the protein complex that when opened through receptor activation allows cation flow across the plasma membrane (Traynelis et al. 2010). mGluRs, on the other hand, do not have an ion channel but usually act through G-proteins (Nicoletti et al. 2011).

The family of glutamate receptors is well-known and widely studied because they are linked to a wide array of essential neuronal functions, such as learning and memory (Nakazawa et al. 2002, Citri & Malenka 2008). They have also been associated with many disorders, for example epilepsy (Waxman & Lynch 2005, Kalia et al. 2008), stroke (Kalia et al. 2008), anxiety disorders (Alt et al. 2006), and migraine (Sang et al. 2004).

2.1.1 Ionotropic glutamate receptors

The sub-family of iGluRs is divided to three classes: kainate, (S)-2-amino3-(3-hydroxy-5-methyl-4-isoxazolyl) propionic acid (AMPA), and *N*-methyl-D-aspartic acid (NMDA) receptors (Traynelis et al. 2010). The grouping is based on ligand-binding properties as well as differences in the sequences of the various receptor classes and the fact that each type of receptor subunit only oligomerizes with other subunit of the same receptor class. The detailed crystal structure of the nearly full iGluR, with only the intracellular C-terminal missing, was not until relatively recently solved (Sobolevsky et al. 2009). This antagonist-bound tetrameric GluA2 revealed the subunit arrangement and symmetry of iGluRs, and how they are connected to each other.

All iGluRs are tetrameric membrane proteins with each monomer consisting of four domains: (1) Extracellular amino-terminal (ATD) affects, for example, sub-class specific assembly and desensitisation of the receptor. However, this is thought to be non-essential for iGluR function. (2) Ligand binding domain (LBD) is the site where the neurotransmitter binds and the consequential conformational changes at the LBD lead to receptor activation and ion channel opening. (3) Transmembrane domain (TMD) has four helices that in the tetrameric complex together form the ion channel permissive to positively charged ions. (4) Intracellular carboxyl-terminal domain affects, for example, membrane targeting of the receptor. It also has phosphorylation sites and binding sites for other intracellular proteins. The full tetrameric structure of iGluRs is organised as a dimer of dimers, with both ATD and LBD domains pairing with equivalent domain from another monomer (Fig. 1A) (Sobolevsky et al. 2009). The domain pairs for ATD and LBD are from different monomers, thus resulting in the extracellular part of the receptor being entwined.

Kainate receptor subunits (GluK1-5) occur in neurons typically as heteromeric receptors and can produce both slow and fast gating kinetics (Traynelis et al. 2010). AMPA subunits (GluA1-4) exist as heteromeric receptors and are specialised in the fast neurotransmission in mammalian brains (Dingledine et al. 1999). Both kainate and AMPA class receptors, however, are also functional as homomeric receptors in recombinant systems (Traynelis et al. 2010). NMDA receptors (subunits GluN1, GluN2A–D, and GluN3A–B) consist of two GluN1 subunits with two other subunits, either of GluN2 or GluN3 type. The NMDA receptors differ from the AMPA and kainate in that they exhibit slower kinetics in both activation and deactivation of the receptor (Monyer et al. 1992, Wyllie et al. 1998, Vicini et al. 1998). Similarly, the NMDA reseptors enter the desensitization state slower than the AMPA and kainate subunits (Dingledine et al. 1999, Traynelis et al. 2010). In addition, there is a Mg^{2+} block in the ion channel of NMDA receptors preventing the passage of ions (Mayer et al. 1984, Nowak et al. 1984). This voltage-dependent block associated with cellular mechanisms of learning and memory is released after the membrane is depolarised by the more rapidly activated AMPA and kainate receptors (Traynelis et al. 2010). Another way to release the block, not related to depolarisation, is by modulating the interactions between membrane lipids and the receptor (Parnas et al. 2009).

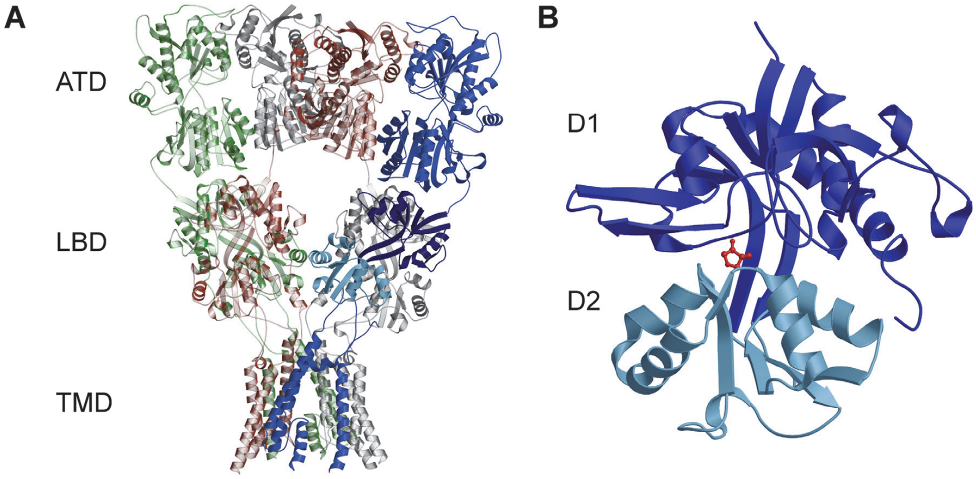

FIGURE 1 Ionotropic glutamate receptor (iGluR) structure. A. Tetrameric structure of iGluR (PDB: 3KG2), showing the extracellular amino-terminal domain (ATD) and the ligand-binding domain (LBD), as well as the transmembrane domain (TMD). Four monomers are each depicted with a different colour. One of the monomers is coloured with different shades of blue to highlight the LBD. Intracellular carboxyl-terminal domain is missing from the structure. B. GluN1-LBD (PDB: 1PB9) with bound partial agonist D-cycloserine (red). Domains 1 and 2 (D1 and D2) of LBD are depicted with different shades of blue (similarly as in A).

2.1.2 Ligand-binding domain structure and activation

All iGluRs are activated by the binding of an agonist to the extracellular LBD. The LBD is composed of two TMD-linked amino acid segments termed S1 and S2. These segments entwine to form the two functional subdomains, D1 and D2, of the LBD. The structure of LBD resembles a clamshell with two β-strands between D1 and D2 serving as a hinge (Fig. 1B) (Armstrong et al. 1998). The binding site for the ligands is located in the cleft between the domains (Sobolevsky et al. 2009). To study the ligand-binding properties of LBD, it can be isolated from the rest of the receptor monomer by cutting the LBD from ATD and TMD and joining the excised S1 and S2 with an artificial peptide linker. The isolated LBD has been demonstrated to show a similar ligand-binding affinity when compared to the wild-type receptor, emphasising the semiautonomous nature of the domain (Kuusinen et al. 1995, Furukawa & Gouaux 2003, Inanobe et al. 2005).

For kainate and AMPA receptors, binding of a natural neurotransmitter L-glutamate to LBD triggers the activation of the receptor by closing the LBD. The opening of the ion channel follows, and (at normal resting membrane potentials) cations can flow through it inside the cell. In contrast to the other two iGluR classes, NMDA receptors (subunits GluN1-3) require binding of both L-glutamate (GluN2) and glycine (GluN1 and GluN3) to be activated (Furukawa et al. 2005). In addition, at least under non-physiological conditions, all four subunits must bind a ligand in order for the ion channel to open (Schorge et al. 2005). The agonists of iGluRs in general share similar chemical groups, namely the α-amino and α-carboxyl, that correspond to those of L-glutamate and are crucial for the ligand-receptor interaction. The residues of LBD directly in contact with these moieties are conserved in the AMPA (Armstrong et al. 1998, Armstrong & Gouaux 2000, Pentikäinen et al. 2003) and GluN2 receptors (Chen et al. 2005, Kinarsky et al. 2005, Erreger et al. 2007). However, GluN1 and kainate receptors show some variation in their sequences around the binding site, which affects ligand selectivity (Pentikäinen et al. 2003, Furukawa & Gouaux 2003, Mayer 2005). In the case of GluN1, these variations display the selectivity of glycine over L-glutamate for this subunit.

The current perception of the mechanism of ligand binding coupling to ion channel opening underlines the importance of the D2 subdomain movements as the LBD encloses the bound agonist. The D1 of the LBD is thought to remain relatively constrained due to intersubunit back-to-back interface contacts between D1 subdomains from two adjacent LBD monomers (Horning & Mayer 2004, Sobolevsky et al. 2009). D2, on the other hand, is able to move more freely to form interactions with the bound ligand and with D1. This movement supposedly leads to a shift in the linker between D1 and TMD and the rearrangement of the transmembrane segments, which eventually results in the ion channel opening (Furukawa et al. 2005, Mayer 2006, Hansen et al. 2007, Sobolevsky et al. 2009). The agonist binding in the LBD is seen as a series of consecutive steps, with ligand-induced closure of the LBD leading to formation of interdomain contacts that stabilise the closed-cleft stage and affect agonist efficacy (Mayer 2011). Indeed, mutatios designed to disrupt interdomain contacts has been shown to reduce the agonist affinity to LBD, whereas introducing additional contacts increased the affinity (Weston et al. 2006).

There exists a broad array of crystal structures for LBDs in complex with various ligands, both agonists and antagonist. In addition to crystallisation, the ligand-binding induced cleft-closure has been extensively studied with several other experimental methods, such as radioligand binding (Frydenvang et al. 2009), fluorescence resonance energy transfer (Ramanoudjame et al. 2006), electrophysiology (Inanobe et al. 2005, Chen et al. 2008), nuclear magnetic resonance spectroscopy (Ahmed et al. 2013), and site-directed mutagenesis (Weston et al. 2006). Recently, computational methods, especially MD simulations, have been utilised to improve our knowledge on the iGluR family structure and function. For example, the movements of LBD on ligand binding (Kaye et al. 2006, Postila et al. 2010), ligand selectivity (Pentikäinen et al. 2006, Erreger et al. 2007), and the role of water molecules inside the binding cavity (Vijayan et al. 2010) have been studied with MD simulations.

2.1.3 Partial agonism of GluN1

Full agonists of iGluRs induce complete domain closure of the LBD and maximal activation of the receptor. In contrast, many partial agonists of AMPA and kainate receptors only prompt an intermediate closure stage when crystallised with LBD. This partial closure stage is not seen in any NMDA receptor structures in complex with a partial agonist ligand despite the fact their activation potential is lower than with full agonists (Furukawa & Gouaux 2003, Inanobe et al. 2005). Thus, according to crystal structures, the degree of closure for NMDA-LBD does not follow the relative efficacies of the full and partial agonists. Nevertheless, partial agonist binding has been suggested to result in a variation at the D1-D2 hinge region conformation (Inanobe et al. 2005). In the same study, movements of the Trp731 side-chain were proposed to play an important role in how the bound partial agonists affect the LBD closure mechanism. These findings, with GluN1 partial agonists 1-aminocyclopropane-1-carboxylic acid (ACPC) and 1-aminocyclobutane-1-carboxylic acid (ACBC), were supported by MD simulations with D-cycloserine (DCS), another partial agonist GluN1 (Kaye et al. 2006). In this computational study, Kaye et al. showed that DCS is able to move inside the binding cavity and adopt various binding modes, some of which may have an effect on hinge region conformation. Another factor putatively affecting the partial agonism of GluN1 is the intersubunit interaction at the LBD dimer interface: recently, both experimental and computational methods indicated that the residue differences between various GluN2 subunits affect the GluN1-bound DCS efficacy (Dravid et al. 2010).

NMDA receptors are known to be important for many crucial functions related to human neuronal activity, for example, learning and synaptic plasticity (Lisman & McIntyre 2001). Consequently, it is understandable that disorders of these receptors may lead to many pathological states. Diseases related to NMDA receptors include neuropathic pain and schizophrenia, among others (Waxman & Lynch 2005, Kalia et al. 2008, Traynelis et al. 2010). Traditionally, antagonism of NMDA receptors has been studied for the possible new treatment of neurological disorders (Kalia et al. 2008, Ogden & Traynelis 2011). For example, the NMDA antagonist memantine, an ion channel blocker, has shown some effect as a treatment for Alzheimer's (Winblad et al. 2007) and Parkinson's diseases (Aarsland et al. 2009). However, the observation of side effects, such as disrupted cognition, encumbers development of this type of antagonists (Traynelis et al. 2010). In contrast to treatments with antagonists, partial agonists have been suggested to be more advantageous as therapeutics because they do not fully prevent the normal activity of the receptors, instead only suppressing the excessive neuronal activity that may arise during pathological states, for example as a result of an ischaemic insult to the brain (Priestley et al. 1998, Wood et al. 2008, Urwyler et al. 2009). Despite all the studies of partial agonism of GluN1, a solid view of the ligand binding relation to receptor activation has yet to be constructed.

2.2 Filamin A

Actin cytoskeleton is responsible for cell shape maintenance. Dynamical modification of the cytoskeleton requires an association with many actin-binding proteins, for example filamins. Filamins (FLNs) are a family consisting of three proteins (FLNa, b, and c) that are coded by different genes but share a high sequence similarity. All three FLN isoforms are active in human: FLNa and FLNb are ubiquitously expressed while FLNc is mostly expressed in muscle tissue (Stossel et al. 2001). FLNs bind and stabilise the filamentous actin network and link them to the cell membrane. In addition to actin, there are over 90 binding partners for FLNs, such as transmembrane receptors, signalling molecules, and proteins related to cell adhesion and migration (Nakamura et al. 2011). As FLNs are related to numerous cellular activities through their binding partners, it is understandable that mutations in genes coding for FLN isoforms can lead to several congenital anomalies (Unger et al. 2007, Robertson 2005, Fox et al. 1998, Robertson et al. 2003). FLN mutations have also been noted to be connected to certain cancers (Sjoblom et al. 2006).

The structure of FLNa is an extended homodimer organised in a V-shape (Fig. 2). Each 280 kDa monomer consists of an amino terminal domain followed by 24 immunoglobulin-like domains of which the most C-terminal domain is responsible for dimerisation (van der Flier & Sonnenberg 2001). Two flexible calpain-sensitive hinge regions divide the monomers to rod1 (domains 1-15), rod2 (domains 16-23), and the C-terminal dimerisation domain (domain 24) (Gorlin et al. 1990). In addition to the N-terminal acting binding domain, the rod1 of FLNa, with its elongated structure, serves as another actin binding site (Nakamura et al. 2007). Rod2, in contrast, shows a more compactly folded structure and is the main interaction site for the FLN binding partners (Nakamura et al. 2011).

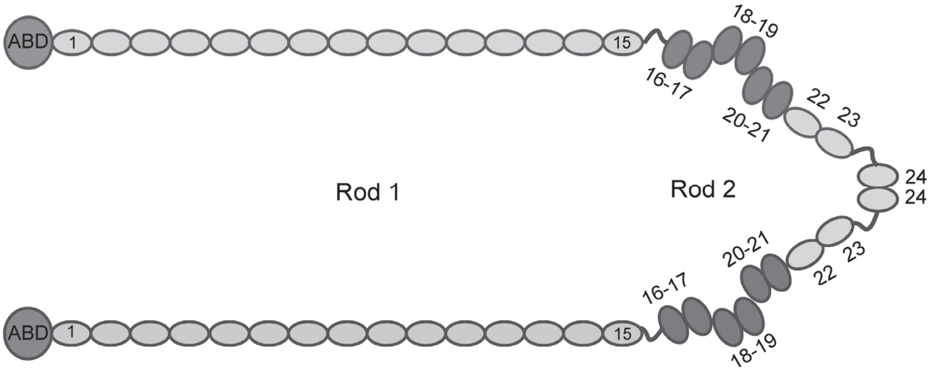

FIGURE 2 Schematic structure of dimeric filamin A structure. Actin binding domain (ABD) is followed by 24 immunoglobulin-like domains. A flexible hinge separates rod1 (domains 1-15) from rod2 (domains 16-23). Another hinge precedes the dimerisation domain (FLNa24). In rod2, domains 16-17, 18-19, and 20-21 are organised as domain pairs (highlighted in dark grey).

2.2.1 FLNa interaction with ligand peptides

Each repeating domain is composed of seven β-strands (named A-G) organised as two antiparallel beta sheets. The general ligand-binding site of FLNa is formed in the groove between strands C and D (so called CD-face), thus allowing interaction partner peptides to bind as an additional β-strand (Fig. 3A). In these binding strands, alternating residues are pointed toward or away from the groove, with the ones facing it restricted to hydrophobic amino acids. The hydrophobic contacts pointed toward strand D, in addition to main-chain hydrogen bonds with strand C, are the main interactions affecting the binding affinity of the partner peptide (Fig. 3B). There is already structural data for many FLNa-peptide complexes sharing this binding mode (Nakamura et al. 2006, Kiema et al. 2006, Lad et al. 2008,). However, there are also many known binding partners for FLNs that do not have a sequence capable of binding as a β-strand, thus suggesting that other binding modes or sites probably exist (Razinia et al. 2012).

The compact configuration seen in the electron micrographs of the FLNa rod2 are a result of domains 16, 18, and 20 pairing with the subsequent odd-numbered domains to form three globular units (Fig. 2) (Lad et al. 2007, Heikkinen et al. 2009). In domain pairs FLNa18-19 and FLNa20-21, the A-strand from the even-numbered domain extends and binds to the CD-face of its odd-numbered pair. This additional strand masks the normal ligand-binding site at the CD-face and probably works as an auto-inhibitor (Lad et al. 2007, Heikkinen et al. 2009). Domains 17 and 23, however, are not auto-inhibited by the A-strands from other domains. Thus, the CD-faces in these two domains are readily available to interact with the partner proteins of FLNa (Heikkinen et al. 2009).

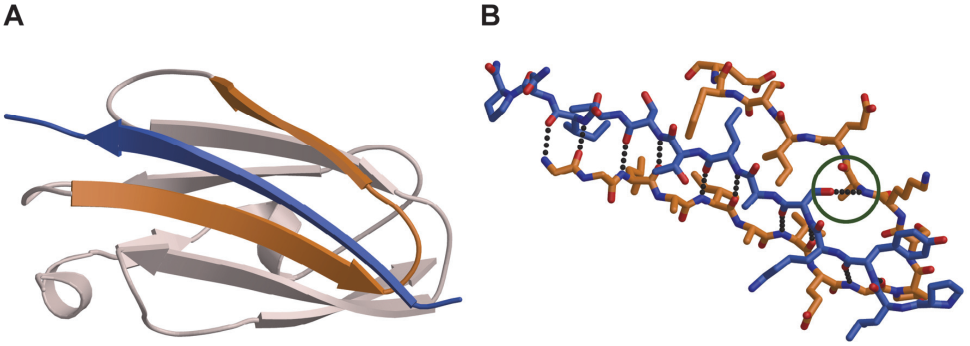

FIGURE 3 Structure of immunoglobulin-like FLNa domain with bound peptide ligand. A. FLNa domains are formed of seven β-strands. Groove between strands C and D (depicted with orange) is the general ligand-binding site. Partner peptides (shown here in blue) bind as additional β-strands. B. Crystal structure of FLNa21 in complex with integrin β7 (PDB: 2BRQ). Hydrogen bonds (dashed lines) between FLNa21 (orange) and integrin β7 (blue) form mostly on the C-strand side. On the D-strand side, hydrophobic interactions prevail, except for Ser780 that forms an H-bond with its side-chain to Ala2281 of FLNa21 (highlighted in a green circle).

As FLNa is an actin cross-linking protein, it is able to serve as a mechanotransducer sensing the mechanical stress in the cytoskeleton (Popowicz et al. 2006, Pentikäinen & Ylänne 2009). It has been shown that FLNa is reversibly unfolded and stretched by external forces (Furuike et al. 2001). These forces, transmitted along the monomers of FLNa, may expose the CD-face for binding partners to attach due to release of the auto-inhibition. In computational simulations with an applied external force, the unmasking has been observed for domain pairs FLNa18-19 and FLNa20-21 (Pentikäinen & Ylänne 2009, Chen et al. 2009). However, it has also been suggested that mechanical stretch is not necessarily a requisite for the release of the auto-inhibition (Ithychanda & Qin 2011, Pentikäinen et al. 2011). It seems that excess ligand peptides, at least in the case of migfilin and filamin, may compete with the masking and release the auto-inhibition. A recent mechanical single-molecule assay supports this view by showing that force facilitated binding of FLNa interaction partners merely shifts the equilibrium of the auto-inhibition (Rognoni et al. 2012).

2.2.2 FLNa domains with a conserved CD-face

Bioinformational studies have suggested that immunoglobulin-like FLNa domains could be divided into four distinct subgroups based on their sequence similarities (Ithychanda et al. 2009). One of these groups contains each odd-numbered domains from rod2 (FLNa17, 19, 21, and 23), and also domains 4, 9, and 12 from rod1. This group, named group A, is of special interest for interaction partner studies as the domains belonging to it share a conserved CD-face. Indeed, all the domains of group A were experimentally demonstrated to bind migfilin, glycoprotein Ibα (GPIbα), and integrin β2 and β7 cytoplasmic tails in similar ways (Ithychanda et al. 2009). In addition, a chloride channel cystic fibrosis transmembrane regulator has been shown to interact with FLNa domains 9, 12, 17, 19, 21, and 23 – that is, all of the group A domains except FLNa4 (Playford et al. 2010, Smith et al. 2010). The GPIbα was shown by isothermal titration calorimetry to bind the group A domains in a micromolar range, with the tightest binding observed with FLNa21 (Ithychanda et al. 2009). GPIbα was also shown to have a higher affinity to FLNa21 when compared to the migfilin and integrin β2 and β7 tails (Ithychanda et al. 2009). According to these quantitative studies, it is possible to rank various FLNa binding partners according to their biding affinities. Considering the fact that FLNs are linked to many disorders, this raises the possibility for designing peptides and peptide mimetics with ideal compositions for binding to FLNa domains.

2.3 T-cell protein tyrosine phosphatase

Opposing actions of phosphatases and kinases regulate many important processes both in eukaryotic and prokaryotic cells. While kinases add a phosphate group to a protein, phosphatases act by removing it. This reversible phosphorylation by kinases and dephosphorylation by phosphatases is traditionally thought to cause their target proteins, for example many enzymes and receptors, to activate and deactivate, respectively. Eukaryotic phosphorylation occurs either with threonine, serine, or tyrosine residue.

Phosphorylation via tyrosine residues is regulated by counteracting protein tyrosine kinases (PTKs) and phosphatases (PTPs). Signalling via tyrosine phosphorylation is known to play a crucial role in many cellular processes such as cell growth and differentiation, motility, and metabolism (Tonks & Neel 2001, Hendriks et al. 2008, Tonks 2013). Proper regulation of these mechanisms is vital, as any failure in the coordination of reversible tyrosine phosphorylation may lead to both acquired and inherent diseases, for example, autoimmune disorders, diabetes, and tumorigenesis (Mustelin et al. 2005, Stuible et al. 2008, Tonks 2013). The family of PTP proteins, encoded by more than 100 genes in the human genome, is responsible for removing phosphate groups from phosphotyrosines (Alonso et al. 2004). Instead of serving only as housekeeping proteins counteracting the PTK action, PTPs are nowadays known to have specific substrate and function specificity and the ability to regulate signal transduction both positively and negatively (Tonks 2006).

TCPTP is an intracellular non-transmembrane PTP. Despite its name referring to T-cells, it is ubiquitously expressed in adult and embryonic tissues (Cool et al. 1989, Mosinger et al. 1992), with the highest expression levels seen in hematopoietic tissues (Bourdeau et al. 2005). There are two splice variants of TCPTP present in humans: the 48 kDa (TC48) and 45 kDa (TC45) forms (Table 1) (Cool et al. 1989, Mosinger et al. 1992). These two isoforms share a conserved catalytical N-terminal, but their non-catalytical C-terminal domains differ. Additionally, the localisation inside the cell is different: while TC48 is targeted to endoplasmic reticulum, the shorter TC45 is present in the nucleus (Lorenzen et al. 1995). However, TC45 is able to exit the nucleus in response to various signals (Tiganis et al. 1998, Lam et al. 2001).

In contrast to general acting PTPs, TCPTP is able to specifically recognise its substrate receptor tyrosine kinases (RTKs) and regulate the signal transduction related to them. The RTKs negatively regulated by TCPTP include several growth factor receptors (Tiganis et al. 1998, Persson et al. 2004, Sangwan et al. 2008), the insulin receptor (Galic et al. 2003), and the colony stimulating factor 1 receptor (Simoncic et al. 2006). For example, the epidermal growth factor receptor (EGFR) is a RTK activated by the binding of an epidermal growth factor. The activation of EGFR leads to TC45 exiting the nucleus and accumulating in cytoplasm (Tiganis et al. 1998). After cell adhesion to collagen by integrins, the $\alpha1$ cytoplasmic tail ($\alpha1$-cyt) of $\alpha1\beta1$ integrin interacts with TC45 and activates it, consequently leading to EGFR dephosphorylation by TCPTP (Mattila et al. 2005). The same $\alpha1$-cyt has been shown to activate TC45 in endothelial cells, resulting in an inhibition of vascular endothelial growth factor receptor 2 activity (Mattila et al. 2008). In addition to RTKs, TC45 isoform is involved, for example, in cytokine signalling pathways via several JAK (Janus kinase) and STAT (signal transducer and activator of transcription) proteins (Simoncic et al. 2002, Aoki &

Matsuda 2002, ten Hoeve et al. 2002, Yamamoto et al. 2002, Lu et al. 2007). Compared to TC45, the TC48 isoform of TCPTP is expressed at lower levels, and as of yet less is known about its function (Muppirala et al. 2013).

The non-catalytic C-terminus of TC45 serves as an auto-inhibiting domain, reducing the activity of the protein by reversibly interacting with the catalytic domain. This has been observed with 33 kDa and 37 kDa (TC33 and TC37, respectively) forms of TCPTP in which the non-catalytic domain is either fully or partially cleaved (Table 1): both of the truncated forms show higher phosphatase activity than the full length TC45 (Cool et al. 1990, Hao et al. 1997). Additionally, the activity of TC33 is inhibited in a concentration-dependent manner if the non-catalytic C-terminal part of TC45 is added (Hao et al. 1997). However, the structure-function studies of the C-terminal of TC45 are hindered by a lack of structural data of this region. The longest available TCPTP structure is missing the last 113 residues from the 387 amino acid long TC45 (Table 1) (Iversen et al. 2002).

TABLE 1 Various isoforms and splice variants of TCPTP.

Name	Lenght aa	Notes	Reference
TC48	415	Natural isoform; Autoinhibited	Cool et al. 1989
TC45	387	Natural isoform; Autoinhibited	Mosinger et al. 1992
TC37	317	Constitutively active; C-terminal truncated	Cool et al. 1990
TC33	288	Constitutively active; C-terminal truncated	Hao et al. 1997
PDB: 1L8K	274	Longest available crystal structure of TCPTP	Iversen et al. 2002

The activation of TC45 by α1-cyt is proposed to stem from the alleviation of the intramolecular auto-inhibition of TCPTP by the binding α1-cyt peptide (Mattila et al. 2005). According to this view, the α1-cyt binds to the N-terminal part of the protein, precluding the autoregulatory interaction between the N- and C-terminals. In a recent high-throughput assay, six TCPTP agonists were identified (Mattila et al. 2010). Two of these, spermidine and mitoxantrone, were found to compete with α1-cyt for binding to TC45 in a concentration-dependent manner. This suggests that they all activate TC45 by binding to the same site. Indeed, like α1-cyt, mitoxantrone and spermidine are also positively charged, which further supports the view.

As TCPTP is a negative regulator of many cancer-related RTKs and is also known to be linked to autoimmune diseases, it would be desirable to develop specific and effective activators for it. Especially promising is the finding that, in contrast to many other phosphatase tumor suppressors, the expression levels of TCPTP are not down-regulated in malignant cells (Lu et al. 2007). Even though mitoxantrone and spermidine are known activators of TCPTP, they are not suitable as therapeutics because they have other targets in cells. In addition, the membrane permeability of these molecules might be restricted due to their charged nature. However, they might be helpful in studies of TCPTP structure and function, and may provide a template for the rational design of TCPTP-specific activators.

3 AIMS OF THE STUDY

Understanding the protein-ligand interaction at the atomic-level is important for future drug design. Accordingly, the aim of this thesis was to investigate three pharmacologically interesting protein targets for their interaction with ligands by using mostly computational methods. The specific aims for each of these projects were revised and sharpened over time. The final aims of the thesis were:

I The aim of the study of iGluRs was to advance the understanding of the partial agonism of these receptors. LBDs of various iGluR subtypes, especially GluN1, were the target to be investigated by using MD simulations. Another aim was to study the energetic basis of the LBD closure with MM-GBSA. It is hoped these studies would facilitate the development of new therapeutic agents for iGluRs.

II The aim of the study of FLNa was to investigate if MM-GBSA based binding free energy calculations could be used to reliably estimate the binding affinities between FLNa and its various peptide-ligands. Constrained MD simulations were aimed to pinpoint the critical interactions in the FLNa-ligand binding.

III The aim of the TCPTP study was to recognise a binding site in TCPTP for mitoxantrone, a novel activator identified by our collaborators. By applying both computational and experimental methods, we aimed to characterise the binding and recognise the structural determinants important for the novel activators of this anti-cancer target protein.

4 METHODS

4.1 Databases

The crystal structures used in the studies reported in this thesis were acquired from the Protein Data Bank (PDB) (Berman et al. 2000). The amino acid sequences were obtained from UniProt (UniProt Consortium 2013).

4.2 Homology modeling

When there were no experimentally solved structures available, or if part of the protein structure was missing from the structure, homology models were built (I, II, IV). Similarly, homology modelling was used in cases when it was necessary to utilise proteins with similar folding (III). The template structures were aligned with the amino acid sequences using MALIGN in BODIL (Lehtonen et al. 2004). Based on these alignments, the models were built using NEST in JACKAL (Petrey et al. 2003) or MODELLER9 (Sali & Blundell 1993). The stereochemical quality of the models was verified with Ramachandran plots (III) acquired with PROCHECK (Laskowski et al. 1993).

4.3 Ligand molecules

The 3D structures for small-molecule ligands (I, II, IV) were prepared with SYBYL7.3 (Tripos International, St. Louis, MO) and optimised quantum mechanically with GAUSSIAN03 (Gaussian Inc., Wallingford, CT) at the HF/6-31+G* level using a polarisable continuum model. The restrained electrostatic potential methodology was used to calculate the atom-centred point charges from the electrostatic potential (Bayly & Kollman 1993). When the studied small-molecule ligand had been crystallised with the protein, the conformation of the ligand was obtained from the crystal structure without geometry optimisation (I, II). The same was applied in cases when peptides were used as ligand molecules (III). The length of the filamin-bound peptide-ligands was unified to 11 residues. With migfilin, this required homology modeling by using an alignment of migfilin sequence (Uniprot: FBLI1_HUMAN) and the structure of integrin β7-bound FLNa21 (PDB: 2BRQ). For experimental studies (IV), molecules were purchased from Sigma Aldrich.

4.4 Structure comparison and ligand positioning

For structure comparison and ligand positioning (I-III), Cα atoms of the target structure and the studied protein-ligand complex were superimposed using VERTAA in BODIL. In addition to superimposition of proteins, peptide-ligands in the study related to filamins (III) were superimposed to attain the same starting conformation for all filamin-peptide complexes. Flexible docking with GOLD 5.0.1 (Jones et al. 1995, Jones et al. 1997) was utilised to identify the putative binding site for mitoxantrone in TCPTP (IV). Docking was also used to predict the bioactive conformations for all the ligands in the same study.

4.5 Molecular dynamics simulations

In MD simulations, the time-dependent behavior of atoms and molecules is mathematically calculated to obtain a detailed view of the atomic motion. Due to the fact that there are usually thousands of atoms in one protein molecule, quantum-mechanical calculations for the whole system are practically inconceivable with current technology. This is further complicated by a box of water molecules in which the protein is embedded for more accurate simulation of real biological environment. Resulting from these challenges, biomolecules such as proteins are commonly simulated using empirical force fields that define the parameters and mathematical equations required for approximation of actual atomic forces in the system. In contrast to quantum mechanical approach, force fields utilise classical Newtonian mechanics to simulate the system. However, small-molecule ligands may still be optimised quantum mechanically prior to docking or inserting into the binding site of the protein for the force-field based MD simulation.

In MD simulations of proteins and their ligands, the molecules are allowed to interact for a certain period of time in a defined temperature. MD simulations yield atomic trajectories that describe the positions, accelerations and velocities of each particle in the course of the simulation. This computational method enables insights into many biological interactions intractable or even impossible to study experimentally. In the studies constituting this thesis, both constraint-free and steered MD simulations were applied to study protein-ligand interactions. For example changes in the distances and angles between atoms of interest were calculated from the trajectories to study the conformational changes occurring as a ligand is bound to a protein. MD was also utilised to study the stability of protein-ligand complexes, and also to mimic the putative forces affecting the protein *in vivo*. Additional utility of MD simulations was to serve as a basis for calculations of binding free energies for protein-ligand complexes.

4.5.1 Constraint-free molecular dynamics simulations

All MD simulations (I-IV) were performed with NAMD2.6 (Phillips et al. 2005) using Amber ff03 force field. TLEAP in ANTECHAMBER-1.27 (Wang et al. 2006) was used to (1) solvate the system with a rectangular box of transferable intermolecular potential three-point (TIP3P) water molecules, (2) add hydrogen atoms, and (3) add counterions (Na^+ or Cl^-) to neutralise the protein-ligand complex. Unnecessary amino acid chains and ions were removed from the crystal structures using BODIL. In studies related to iGluRs (I, II), the extra water molecules too close (1.4 Å) to the ligand were removed if the original protein-ligand complex from a crystal structure was not used directly. In addition, in these studies the disulphide bridges were built between adjacent cysteine residues (GluN1: Cys420-Cys454, Cys436-Cys455, and Cys744-Cys798).

The MD simulations were performed in four steps in order to energy minimise and equilibrate the system before the product simulation. First, the energy minimisation of the water molecules, counterions, and amino acid side chains was done while the rest of the system was kept constrained by restraining Cα atoms with a harmonic force of 5 $kcal*mol^{-1}*Å^{-2}$. In the second step, energy minimisation for the whole system was performed without constraints. Third step was a MD simulation run with restrained Cα atoms in a constant pressure. Finally, the actual production MD simulation with no constraints was performed, with the length of the run ranging from 6 to 127 ns depending on the study. Usually three repeats were performed for each studied complex.

During the MD simulations, the temperature was kept at 300 K with Langevin dynamics for all non-hydrogen atoms using a Langevin damping coefficient of 5 ps^{-1}. Nosé-Hoover Langevin piston (Feller & Pastor 1995) was utilised to keep the pressure at 1 atm with an oscillation time scale of 200 fs and a damping time scale of 100 fs. An integration time step of 2 fs was used under a multiple time stepping scheme (Schlick & Schulten 1999). In general, the bonded and short-range interactions were calculated every step and long range electrostatic interactions every third step. A cutoff value of 12 Å was used for the short-range electrostatic interactions and van der Waals forces, and a switching function was enforced for the van der Waals forces to smoothen the cutoff. The simulations were run under periodic boundary conditions, and the long-range electrostatics were counted with the particle mesh-Ewald method (Darden & Pedersen 1993). The hydrogen bonds were restrained with the SHAKE algorithm (Ryckaert & Berendsen 1977).

Trajectory analysis of MD simulations was done by extracting snapshots at specific intervals from the trajectories with PTRAJ in ANTECHAMBER 1.27

(Wang et al. 2006). Various atom distances and angles, as well as calculation of RMSD values of ligands, were measured using the trajectories. A cutoff value 3.4 was used as the upper limit for a hydrogen bonding distance. Visual inspection of snapshots was performed with BODIL.

4.5.2 Steered molecular dynamics simulations

In steered molecular dynamics (SMD), an external force is added to force fields to allow mimicking of the effects of mechanical strain on the studied molecules. With the usage of external forces, SMD accelerates conformational changes in the system by reducing energy barriers. This application broadens the repertoire of subjects possible to study with MD simulations. In SMD, one or multiple atoms are kept fixed while an external force is added to others. Constant force or constant velocity schemes may be applied depending on the study.

In the studies constituting this thesis, a constant force was applied to the center of mass of the Cα atoms of D2 of GluN1-LBD (II) or to filamin-bound peptides (III). The atoms that were kept fixed were either the Cα atoms of D1 of GluN1-LBD (II) or Cα atoms of filamin domain (III). The direction of the force was defined by the vector linking the center of mass of the fixed and constrained atoms. Various forces in the piconewton range (from 6 to 200 pN) were applied depending on the study. The SMD simulations followed the protocol reported for MD simulations except that the SMD productions runs were performed only after short unrestrained MD simulations. Another alteration was that the time step used in the SMD simulations was 1 fs compared to 2 fs in the constraint-free runs.

4.6 MM-GBSA

Estimation of binding free energy (ΔG_{bind}) is essential for many studies of biological interactions. For example, drug discovery processes such as virtual screening can be assisted by the free energy calculations with small molecules (Niinivehmas et al. 2011). Other examples of applications that can be advanced with the help of ΔG_{bind} estimations include ranking both small-molecule (Hou et al. 2011) and peptide ligands (Zuo et al. 2012) on the grounds of their binding affinity. Yet another valuable application of binding free energy methods is to investigate the energetic basis of protein conformation changes (Fogolari et al. 2005, Tomic et al. 2012).

MM-PBSA/GBSA method, originally applied to study nucleic acids (Srinivasan et al. 1998), combines the molecular mechanical approach with the desolvation energies to estimate free energies of binding. The method has been shown to be efficient in predicting the energetics of ligand binding to proteins (Massova & Kollman 2000, Rastelli et al. 2010). In contrast to the explicit water model generally used in MD simulations, continuum solvent models of Poisson Boltzmann (PB) or Generalised Born (GP) are utilised in MM-PBSA/GBSA to estimate the electrostatic contribution to the solvation free energy. Use of a continuum model of the dielectric properties of water is obviously only an approximation of the actual solution environment. However, it notably reduces the computational cost of the calculations and makes the equilibration step for water redundant. In the studies (II-IV) constituting this thesis, GB model was utilised as it has been shown that it is usually better in ranking the binding affinities of the ligands compared to PB model (Hou et al. 2011).

In MM-GBSA, the binding free energy between a ligand and a protein is estimated from the free energies of the complex, protein, and ligand with the following equation:

$$\Delta G_{bind} = G_{complex} - G_{protein} - G_{ligand}$$

The free energy for each species is estimated from the molecular mechanics energies (E_{MM}), solvation energies (G_{sol}), and the entropic term (TS_{solute}) using the equation:

$$G = E_{MM} + G_{sol} + TS_{solute}$$

where E_{MM} is the sum of van der Waals (E_{vdw}), electrostatic (E_{elec}), and internal energies (E_{int}) in vacuo. G_{sol} in turn presents the solvation free energies including both the polar (G_{GB}) and nonpolar (G_{SA}) components. The free energies of binding were estimated from MD simulation trajectories using the MM-GBSA method implemented in AMBER10 (Case et al. 2008). E_{MM} was calculated with sander program from AMBER with infinite cutoff. G_{GB} was calculated with GB approach implemented in AMBER. There are three different GB models offered in the Amber10 package: IGB1 (Hawkins et al. 1996, Tsui & Case 2001), IGB2, and IGB5 (Onufriev et al. 2004). Of these, either only IGB1 (II, IV) or all of them (III) were used in MM-GBSA calculations. Solvate accessible surface area for the G_{SA} was determined using MOLSURF (Connolly 1983), and the surface tension constants used were 0.072 for IGB1 and 0.005 for IGB2 and IGB5. Dielectric constants of 1 and 80 were used for solute and solvent, respectively. The conformation entropy term (TS_{solute}) was not considered here as it has been shown that the entropic configuration calculations are often unreasonable (Gohlke & Case 2004), and are not essential for the ranking of binding affinities of similar ligands (Hou et al. 2011). The ΔG_{bind} values shown for each protein-ligand complex were calculated as averages from snapshots taken from MD simulation trajectories at 6 ps (III) or 120 ps (II, IV) intervals.

4.7 Experimental methods

4.7.1 Isothermal titration calorimetry

Isothermal titration calorimetry (ITC) is an experimental method capable of providing quantitative information about the energetics of biological interactions (Velazquez-Campoy et al. 2004). It enables a detailed determination of several thermodynamic parameters in a single measurement, such as ΔG, enthalpy (ΔH), entropy (ΔS), and dissociation constant (K_d). In addition, kinetic parameters of biomolecular reactions have also been shown to be determinable by using ITC (Egawa et al. 2007). The basic protocol is to inject the ligand in aliquots in to the sample (protein) solution and to measure the power required to maintain a constant temperature compared to a reference solution in an adjacent chamber. Energy is either released or taken up after each injection, so the feedback system of the calorimetry has to either raise or lower the thermal power applied to reach the equilibrium. As the titration progresses, all the binding sites are gradually vacated and, consequently, the heat signal diminishes. The ΔH, K_d, and the stoichiometry can be defined from the binding isotherm produced. Accordingly, also the ΔG and the entropic contribution to the event ($-T\Delta S$) can be judged.

Here, the ITC was utilised to study the small-molecule activators binding to TCPTP (IV). ITC200 calorimeter (GE Healthcare Life Sciences, Microcal Inc.) was used for mitoxantrone-TCPTP complex and VP-ITC (GE Healthcare Life Sciences, Microcal Inc.) for spermidine-bound TCPTP. In measurements of mitoxantrone binding, HEPES buffer (50 mM HEPES, 150 mM NaCl, 10 mM β-mercaptoethanol), pH 7.0, was used with the concentrations of 20 μM and 200 μM of protein and ligand, respectively. The titration was carried out with 3 μl aliquots with two minute intervals. For spermidine, Tris buffer (20 mM Tris, 100 mM NaCl, 10 mM β-mercaptoethanol), pH 8.0, was used, and the concentrations of the reactants were 15 μM for spermidine and 300 μM for TCPTP. Volume of the injections here was 15 μl with four minute intervals. Data analyses was done with Microcal Origin 7.0 (MicroCal LLC) software.

4.7.2 Differential scanning fluorimetry

Differential scanning fluorimetry (DSF) enables assessing the effect of a ligand on the temperature-dependent protein melting (Pantoliano et al. 2001). In DSF, a hydrophobic fluorescent dye is utilised to differentiate between folded and unfolded protein conformations. At low temperatures, no signal is detected because there are no hydrophobic core-residues exposed to which the fluorescent dye could attach. However, as the temperature is gradually raised, protein starts to unfold and the dye is able to bind to emerging hydrophobic surface patches. The fluorescence signal is read, and the melting temperature (T_m) of the protein complex is calculated from the resulting fluorescence curve. The effect of ligand-binding to the conformational stability of a protein can be estimated by comparing the T_m values of the protein with or without a bound ligand.

Here, DSF was used to study the stability and folding of various TCPTP constructs and the effect of small-molecule activators on the T_m of the constructs (IV). Assays were performed with Bio-Rad C1000 Thermal cycler (CFx96 Real-Time System), and SYPRO Orange (Invitrogen) was used as the fluorescent dye. Temperature increments of 0.5 °C / 30 s from 20 °C to 95 °C were applied in all experiments. Concentrations of 10 and 100 µM were used for protein and ligand, respectively, and the SYPRO Orange dye was diluted to 5x concentration for the final samples. HEPES buffer (50 mM HEPES, 150 mM NaCl, 10 mM β-mercaptoethanol), pH 7.0, was used in the assays, and the total volume of the samples was 25 µl. In contrast to mitoxantrone and spermidine, 1,2-diaminoanthraquinone was diluted in DMSO. Hence, the same DMSO concentration was used in the ligand-free protein samples to which the effect of 1,2-diaminoanthraquinone was compared. Four parallel measurements were performed and the average numerical results were calculated based on them.

4.7.3 Other experimental methods utilised

Recombinant TC37 and TC45 cloning, expression and purification was performed as described in detail in the corresponding publication (IV). Surface plasmon resonance assay and pull-down, as well as the phosphatase assays, were conducted by our collaborators (IV).

4.8 Visualisation

Figures showing structures of proteins or protein-ligand interaction were generated with BODIL v. 0.81 and MOLSCRIPT v. 2.1.2 (Kraulis 1991) and rendered with RASTER3D v. 2.7C (Merritt & Bacon 1997).

5 RESULTS

5.1 Ionotropic glutamate receptors (I, II)

In contrast to immobile crystal structures, MD simulations enable a dynamic study of the events taking place between iGluRs and binding ligands. It was shown in a former study (Postila et al. 2010) that MD simulations can distinguish between the agonists and antagonists, and perhaps also partial agonists, of GluK1, and reproduce similar closure-stages seen with experimental methods. To expand this research, a large set of full and partial agonists were inserted to the LBD of GluK2, GluA2, and GluN1 receptors, and constraint-free MD simulations were run to study the closure stages of the cleft and the critical interactions between the ligand and the receptor (I). Partial agonism of the GluN1 was of particular interest, and therefore it was studied more thoroughly: the forces from the transmembrane domain of GluN1 that likely apply to LBD were mimicked by SMD simulations, and the energetic basis of the ligand-binding interactions was estimated using the MD-based MM-GBSA (II).

5.1.1 Interdomain H-bond efficiently indicates cleft closure (I)

Several interdomain distances were measured from MD simulation trajectories to see if the effect of full and partial agonist binding to the cleft closure could be differentiated. One particular H-bond (Gly485^{N}-Gln686^{O} for GluN1; Gly472^{N}-Ser673^{O} for GluA2; Gly489^{N}-Asp687^{O} for GluK2), located between the D1 and D2 of LBD, was found to correlate especially well with the partial agonism of iGluRs (I, Fig. 3): With full agonists, this interdomain hydrogen bond (IHB) was formed and remained stable during the MD-simulations. Partial agonists, on the other hand, consistently disrupted the bond. Thus, IHB was focused when the MD simulations were inspected and the closure of the LBD was analysed. In addition to IHB measurements, iGluR-LBD closure angles were also calculated by using three different triangles. However, due to the fact that with this method the relative position of three atoms needs to be considered, none of the triangles described the closure of the binding-cleft as reliably as the IHB distance calculations (I, Fig. S2).

5.1.2 Full agonists maintain the LBD closed in MD simulations (I)

When simulated with bound full agonists, the LBDs of GluA2 and GluN1 were kept firmly closed (I, Fig. 4B, 6B and S3, Table S2 and S5). However, this was not constantly seen with GluK2: the IHB broke from time to time in most of the repeats (I, Fig. 5B and S3, Table S3). Thus, unlike GluN1 and GluA2 and at least in simulations of isolated LBDs, GluK2 seems to be prone to opening even with bound full agonist ligands.

5.1.3 Partial agonists destabilise closed-cleft iGluRs (I)

The effect of partial agonists on the closure of GluA2 was studied with 5-substituted willardiines. The ligands, when inserted in a closed-cleft LBD, temporarily broke the IHB (I, Fig. 4 and S3). However, the cleft did not stay open constantly in any of the simulations, indicating that incomplete closure of GluA2-LBD may not be essential for partial agonism in this receptor type.

In simulations of GluK2, bulky partial agonists kainate and domoate invariably opened the LBD to the same intermediately open stage as seen in crystal structures (I, Fig. 5 and S3). However, with kainate the IHB temporarily formed (I, Fig. S3) in some simulations, suggesting that in addition to the intermediate closure stage, the GluK2-LBD is also able to fully close with bulky partial agonists.

In contrast to what is visible in the crystal structures of GluN1-LBD with bound partial agonists, the MD simulations showed that the cleft can be opened with these ligands (I, Fig. 6 and Table S5). While full agonists glycine and D-serine kept the LBD firmly closed, partial agonists D-cycloserine and ACPC broke the IHB and opened the binding-cleft similarly, as seen with GluA2 and GluK2.

In summary, not all partial agonists of GluA2 or GluN1 were able to open the fully closed LBD. However, they were capable of breaking the IHB, thus suggesting that this bond plays a crucial role in the partial agonism of these receptors. The GluK2 subtype, on the other hand, did not allow a clear distinction between full and partial agonists.

5.1.4 MD simulations reveal an intermediate closure stage for GluN1 (I, II)

When the simulations of GluN1 with bound partial agonist D-cycloserine (I, Fig. 6) were analysed, a relatively stable plateau was noticed in the IHB distance calculations around 4-5 Å. This distance was clearly longer than the H-bond in closed-cleft but shorter than what is seen in the crystal structures of the fully open GluN1-LBD. To further study this previously unseen closure stage, MD simulations with full and partial agonists inserted to open-stage GluN1-LBD (from an antagonist-bound crystal structure) were run. With full agonist glycine and relative small partial agonists D-serine and ACPC, closure of the LBD was repeatedly induced, but with bulkier ACBC this did not occur. However, when the IHB distance was measured, an intermediate closure stage was visible with all the partial agonist in the course of the simulations (II, Fig. 2 and S1). This partial closure stage was stable, lasting several nanoseconds in each simulation run with every partial agonist studied. In some repeats, full closure of the cleft followed the intermediate closure, but in other cases complete closure was not achieved at all. For D-cycloserine, the IHB distance at the intermediate closure stage was approximately 4-5 Å, resembling what was noticed in simulations from a closed-cleft conformation of LBD (I, Fig. 4). For ACPC and ACBC, the IHB distance was 5-6 Å when the intermediate closure stage was reached. In addition, with ACBC another partial closure stage was also seen at 4-5 Å (II, Fig. S1). Contrary to partial agonists, full agonist glycine did not show intermediate closure stage in any of the simulation runs.

5.1.5 SMD simulations mimic forces affecting the GluN1-LBD closure (II)

To study the strength of the full or partial agonist-bound GluN1-LBD closure, SMD simulations were run. The D1 lobe of the LBD was kept fixed while constant forces, ranging from 6-10 pN, were applied to the Cα atoms of D2 (II, Fig. 3 and S2). The direction of the force was from the centre of the mass of Cα atoms D1 towards that of D2. The starting structure of the LBD was fully closed (obtained from a crystal structure with bound full agonist glycine), so the forces likely affecting the opening of the LBD *in vivo* could be mimicked. With full agonist glycine, the forces needed to open the closed-cleft LBD were higher than with partial agonists D-cycloserine, ACPC, and ACBC. This was observed when the IHB distance was measured from SMD simulation trajectories: 9-10 pN was needed to wedge the glycine-bound LBD open while smaller forces, even as low as 6 pN, were enough to open partial agonist-bound complexes (II, Fig. S2).

With all partial agonists, the IHB distance in the SMD simulations were set to the same intermediate stage as seen in the constraint-free MD runs (II, Fig. 3 and S2). In some repeats, this partial closure persisted for the whole 3 ns simulations, while in others the LBD opened fully in the later stages of the simulation. Similarly as with free-MD simulations, full agonist glycine did not show intermediate closure but opened completely with no stable partially open stage. Average IHB distances at the intermediate closure stage correspond to some extend with the previous experimental results of ligand efficacies (Inanobe 2005, Priestley 1995): the most effective partial agonist D-cycloserine showed the shortest IHB distance at the intermediate closure level, while ACBC with the lowest reported efficacy had the longest distance.

5.1.6 Closure mechanism of GluN1-LBD (II)

The mechanism of closure of GluN1-LBD was examined from MD simulations starting from an open-cleft structure. Various distances from different sides of the GluN1-LBD binding cavity were measured from trajectories of MD simulations with either a full or partial agonist bound. It was noticed that the closure of the cleft does not take place simultaneously throughout the binding cavity: the H-bond between Gln405^{OE1} and Trp731^{NE1} near α-helixes H and I forms earlier than the IHB on the other side of the cavity (II, Fig. 4B and S3). In addition, there was no intermediate closure stage visible in the distance plots of the Gln405-Trp731 obtained from the partial agonist simulations. The same observation was made when snapshots were extracted from MD simulation trajectories: while three distinct closure stages are visible at the area close to the IHB (near helix F and loop 2), only two stages are seen at the other end of the binding cleft (II, Fig. 4C).

5.1.7 Energetic basis of the GluN1-LBD closure (II)

To study the ligand-binding energetics associated with different closure stages of GluN1-LBD, MM-GBSA was utilised. The binding free energies were estimated from trajectories of MD and SMD simulations. With full agonist glycine, there was a clear decrease in the ΔG_{bind} when the open-cleft LBD closed during the MD simulation (II, Fig. 3). When simulated from the closed-cleft conformation, no change in the ΔG_{bind} level was seen. In SMD, the binding free energy clearly followed the opening of the LBD. In summary, MM-GBSA calculations with glycine-bound GluN1-LBD showed that full agonists noticeably prefer the closed-cleft form of LBD.

When trajectories of GluN1 with bound D-cycloserine were analysed, it was noted that there is little or no difference between the fully or partially closed stages in the binding free energy levels (II, Fig. 3). In SMD runs, the ΔG_{bind} differed at the intermediate closure stage slightly from that seen at the fully closed stage. However, later during the same run, as the LBD fully opened, a more significant change in the energy level was visible. Similar results were obtained in SMD simulations with ACPC and ACBC (II, Fig. S3). Hence, MM-GBSA results depict that the full closure of the GluN1-LBD is not clearly the energetically favored conformqation when compared to intermediately closed LBD. The numerical results from the MM-GBSA calculations of SMD simulations were correlated well with the EC_{50} values reported earlier (Chen 2008, Dravid 2010, Priestley 1995) with experimental methods (II, Table 1).

5.2 Filamin A interaction with peptide-ligands (III)

Interaction of peptide-ligands with filamin was studied with computational methods. The aim was to determine the reliability of the *in silico* methods in estimating the binding affinities of peptides to FLNa domains. Binding free energies of peptide-ligand-bound FLNa-domains were calculated with MM-GBSA. Original crystal structures, or, when necessary, homology models, were used as the starting conformations for MD simulations. Binding free energies were estimated from trajectories of the simulations and compared to the experimental results obtained from literature. In addition, SMD was utilised to analyse filamin-ligand interaction at the atom-level. Finally, biological problems related to filamins were studied with MM-GBSA to see if computational methods could illustrate the problems currently not solved by traditional experimental techniques.

5.2.1 Peptide-ligand-bound Filamin A MM-GBSA calculations compared to experimental data

The binding free energies of various FLNa-domains in complex with GPIbα or several binding-partners bound to FLNa21 were calculated using MM-GBSA. After 6 ns constraint-free MD simulations, an average ΔG_{bind} for the filamin-ligand-complex was calculated from 1000 snapshots extracted from the trajectory. Only FLNa domains that are known to share similar binding groove between β-strands C and D were selected for this study. Three different IGB-models were considered for each FLNa-peptide complex.

Binding free energies for various peptides (GPIbα, migfilin, and integrin beta cytoplasmic tails 2 and 7) binding to FLNa21 were calculated with MM-GBSA and compared to the experimental results reported in the literature. High correlations were seen with all three IGB-models: coefficients of determination (R^2) for IGB1, IGB2, and IGB3 were 0.94, 0.96, and 0.96, respectively (III, Fig. 2 and Table 2). When the binding free energies of FLNa domains 9, 12, 17, 19, 21, and 23 in complex with GPIbα were calculated and compared to experimental results, a high correlation was seen with two IGB-models: R^2 of 0.95 and 0.93 were obtained for IGB1 and IGB2, respectively (III, Fig. 2 and Table 1). For IGB5, the correlation was only moderate, 0.62. Also, the standard deviations of IGB5-calculations were larger than with the other two models (III, Table 1). When the binding free energies of individual runs were plotted against the simulation time, a relatively good converging of the energies was noted (III, Fig. S2 and Table S2). Nevertheless, there was a large fluctuation in the energy levels in the case of IGB5, justifying the low correlation and relatively large standard deviation seen in the numerical results. However, when these results were combined in the same plots with the results of FLNa21 bound to various peptides, the correlation was very high regardless of the IGB-model selected (III, Fig. 2).

5.2.2 SMD simulations of FLNa21-peptide complexes

Atom-level analysis of the FLNa21-peptide interaction was performed by SMD simulations. FLNa21 Cα-atoms were kept fixed while a constant force was applied evenly to all Cα-atoms of the bound peptide. Various forces were tested for each binding partner to discover the force needed to detach them. GPIbα was found to require the most force, even 200 pN, to disengage, while the integrin β2 cytoplasmic tail usually needed only 100-150 pN. Visual inspection of the snapshots, extracted at various time points during the SMD simulations, showed that the detaching of all peptides always started from the C-terminal (III, Fig. 3). This was also visible when atom distances between the main chain N- and O-atoms of FLNa21 C-chain and the bound peptide were calculated from the trajectories (III, Fig. 3 and S3). In addition to these interactions, another H-bond was found to play a critical role in the FLNa21-peptide relationship: serine in position 4 for all peptides considered in this study was seen to form a hydrogen bond to Ala2281, located at strand D of FLNa21 (III, Fig. 1). In SMD simulations, this H-bond was always the last to break, indicating the crucial role of this particular interaction for the affinity of the bound ligand-peptide (III, Fig.3 and S3).

5.2.3 FLN-related biological problems studied with MM-GBSA

Autoinhibition of FLNa21 by the A-strand from the adjacent FLNa20 has previously been studied experimentally (Lad et al. 2007, Heikkinen et al. 2009). The binding affinity of the A-strand to the CD-face of FLNa21 was here estimated with MM-GBSA. According to the calculations, based on 1000 snapshots from 6 ns long MD simulations, the ΔG_{bind} for this interaction is at a similar level as the integrin β tails 2 and 7 (III, Table 2). GPIbα and migfilin, on the other hand, showed a significantly higher binding affinity towards FLNa21.

Another biological problem studied with MM-GBSA was the binding of migfilin to chain B of the FLNa21-migfilin complex, which was obtained from the corresponding crystal structure (PDB: 2W0P). Similarly to aforementioned MM-GBSA calculations with the A-strand of FLNa20, 6 ns MD simulations were followed by binding free energy estimations from 1000 snapshots. The ΔG_{bind} result (-70.9 kcal*mol^{-1}) corresponds to an experimental value of -2.4 kcal*mol^{-1} which is considerably lower than that calculated for the FLNa21 A-chain with bound migfilin (III, Table 2).

5.3 T-cell protein tyrosine phosphatase activation by small molecules (IV)

It was known from previous studies that the cytoplasmic tail of α1-integrin (α1-cyt) binds to and activates TCPTP (Mattila et al. 2005). In addition, six small molecules have been identified that are able to activate TCPTP. The aim here was to investigate the mechanism of TCPTP activation and to identify the binding site for the small molecule activator mitoxantrone. For that purpose, mitoxantrone and other small activators were analysed with several experimental and computational methods. In addition to studying the binding and activation of TCPTP with these recently recognised molecules, the activation of the protein with α1-cyt was examined.

First, mitoxantrone and spermidine were studied using ITC for their binding stoichiometry and affinity. The constitutively active form of TCPTP, TC37, was used because it is more stable and soluble than TC45. The binding of mitoxantrone was shown to be exothermic (ΔG_{bind} = -8.1 kcal*mol^{-1}), with both enthalpy and entropy having a favourable effect (IV, Fig. 2). According to the stoichiometry estimation, only one binding site was suggested to exist for mitoxantrone. On the other hand, ITC measurements showed that spermidine does not bind to TC37.

Docking studies were utilised to identify a probable binding site for mitoxantrone. As there are no 3D-structures available for the full-length TC45, a homologous protein (PTP1B) was used as a template to build the TC30 construct. While this model lacks the C-terminal part of the TCPTP, it could be used for docking studies because ITC studies have demonstrated that this part of the protein is not needed for binding. Docking studies revealed a negatively charged area with a hydrophobic groove near the N-terminus of TCPTP, distinct from the catalytic site. This putative binding site provides a favourable environment for the binding of mitoxantrone, which has positively-charged arms as well as a hydrophobic core (IV, Fig. 1 and 3). Verification for this was obtained with MD simulations, which showed that the mitoxantrone docked into this site remains firmly in place (IV, Fig. 4). In contrast, MD simulations with spermidine indicated that it is unable to stay in the binding site during the simulation. This further supports the earlier obtained results with ITC that suggest a different activation mechanism for spermidine.

Two mutant forms of TC30, E8.E11A and E24.28A, were tested to see the effect of these mutations to the mitoxantrone binding. MD simulations of 6 ns were followed by MM-GBSA calculations of free energy for the binding event. The results suggest that mitoxantrone binds more strongly to the wild type TCPTP than either of the mutants. Both glutamate-to-alanine mutations also affect the thermal stability of TCPTP, which was seen when the DSF was utilised to study the thermal denaturation profiles of the constructs. For this, TC45, TC37, and the two mutations were expressed and purified. Compared to the wild type TC37, the E24.28A and especially E8.11A mutants destabilised the *apo*-form of the protein. However, these DSF results confirm the stability of both wild type and mutant constructs. When mitoxantrone was added and the DSF results were compared to experiments with no activator bound (IV, Fig. 5 and Table 2), a small elevation was seen in the T_m-value (+2.1 ^oC). In contrast, a negative effect on the T_m value was noticed with both mutant forms and with the TC45 bound to the mitoxantrone. In the melting curves of mitoxantrone-bound TC37 and both mutant constructs, two distinct transition states were seen, thus proposing that there exists two subdomains in the TC37 structure, of which one is stabilised by mitoxantrone. For 1,2-diaminoanthraquinone, a small positive effect was seen with all protein constructs compared to the *apo*-form (IV, Fig. 5 and Table 2). Spermidine, on the other hand, destabilised all the protein constructs as seen in the negative shift of the T_m-values (IV, Fig. S2 and Table 2).

The phosphatase activity assay indicated that the 1,2-diaminoanthraquinone did not activate TC45 phosphatase action even though it was shown in the DSF measurements to bind and stabilise the protein (IV, Fig. 5 and Table 2). On the contrary, both mitoxantrone and α1-integrin clearly activated the TC45 in the phosphatase assay (IV, Fig. 6). Vigorous activation by α1-cyt was emphasised when it was co-incubated with the mitoxantrone: the addition of mitoxantrone did not produce any additional effects when compared to the α1-cyt alone (IV, Fig. S3). When the effect of double mutants (E8.11A and E24.28A) on the binding and activation of α1-cyt were studied with surface plasmon resonance and pull down and phosphatase assays, only a slight effect was noted (IV, Fig. 7). These findings depict that the double mutations do not completely prevent α1-cyt from binding and activating the TCPTP. The tetra mutant (E8.11.24.28A) form of TC45, however, clearly weakened the binding and hindered activation ability (IV, Fig. 7).

6 DISCUSSION

6.1 Ionotropic glutamate receptors

6.1.1 IHB disruption enables categorisation of ligands as full or partial agonists

MD simulations with LBDs of GluA2 and GluN1 showed that the binding cleft stays firmly closed when in complex with full agonists. However, with GluK2 the cleft can be opened during long MD simulations, indicating a less firm closure when compared to the other two receptor types. In the case of partial agonists, the stability of the IHB correlates well with the ligands and putatively plays a critical role in the partial agonism of GluA2 and GluN1: while some partial agonists were unable to permanently wedge the binding cleft of these receptors open, the IHB was frequently disrupted with all studied partial agonists. These results suggest that categorising the ligands of GluA2 and GluN1 as full or partial agonists could be justifiable based on IHB stability, albeit a larger dataset of different agonists would be required to verify this. GluK2, on the other hand, did not show as clear of a distinction between full and partial agonists, which makes the categorisation of agonists more unreliable for this receptor type. Relatively small ligands can act as GluK2 specific partial agonists, which may arise from the weak link between D1 and D2 of the LBD of this receptor type.

A very recent study (Ahmed et al. 2013), using hydrogen-deuterium exchange method, supports the view of hydrogen bonding stability being important in distinguishing full and partial agnists at least in GluA2. In that study, stabilisation of the interdomain H-bonds was weaker for partial than for full agonists. Similarly, in another recent study (Ahmed et al. 2011), even the very weak agonists of AMPA receptors were seen to induce full closure of the LBD, but only transiently. Thus, it is proposed that it is not the extent of closure in a single state but the relative stability of the various closure stages that determines the efficacy of the ligand (Ramaswamy et al. 2012).

As all iGluRs usually exist as heteromeric complexes, it would be worthwhile to study other iGluR subunits in addition to GluA2, GluK2, and

GluN1 with the same agonists used here. This would yield a complete picture of the pharmacological properties of the ligands.

6.1.2 The mechanism of intermediate closure of GluN1-LBD

The intermediate closure stage for partial agonist-bound GluN1 was observed in free MD simulations starting from a closed and open binding cleft, as well as in SMD simulations from a closed cleft. In addition to IHB distance measurements, the intermediate closure was seen in the superimposition of snapshots from the simulations with crystal structures of GluN1-LBD: the intermediate closure differs clearly from the full agonist and antagonist-bound crystal structures in the cleft openness. The intermediate closure resembles that seen in the AMPA receptor LBD in complex with bound the partial agonists. Furthermore, MM-GBSA calculations revealed that the intermediate closure is a stable conformation and the full closure is not clearly preferred.

It was visible in the MD simulations starting from an open cleft LBD of GluN1 that the closure of the binding cleft does not occur simultaneously at every part of the cavity. The IHB forms slower than the other interdomain bond between Gln405 and Trp731 on the other side of the cavity. A similar phenomenon was seen earlier in GluK1-LBD with a partial agonist 9-deoxy-neoDH (Postila et al. 2010). In the case of GluN1, three distinct closure stages were visible only on the IHB side of the binding site. One putative explanation to this is that contrary to IHB, which is formed between main chain atoms N and O, the Gln405-Trp731 bond forms between side chains of the amino acids, thus allowing them more freedom for small movements. Therefore, the Trp731 side chain may slightly alter its conformation depending on the ligand as suggested previously in a study based on crystal structures (Inanobe et al. 2005). However, the H-bond to Gln405 stays formed despite the small movements, and hence no intermediate closure is seen in the binding cavity near these residues.

Why, then, is this intermediate stage not seen in any crystal structures of partial agonist-bound GluN1? One answer may lie in the static nature of X-ray structures: only one of the possible conformations and permitted motions is seen in crystals. MD simulations, on the other hand, can shed additional light on the iGluR-partial agonist interaction by revealing the dynamics related to the ligand-binding event. Another explanation for the missing intermediate closure stage in crystal structures could be the fact that forces from the TMD cannot be considered in structures of isolated LBDs. In full structures of iGluRs, the D2 of the LBD is closely linked to TMD via the linker between D2 and transmembrane helix TM3. This linker is thought to be critical for gating and it likely transmits conformational dynamics between LBD and TMD (Sobolevsky et al. 2009). Thus, forces from TMD directed to LBD likely transmit via this linker and affect the parts of D2 of the LBD most closely connected to it, for example, the IHB residue Gln686 (II, Fig. 4). This would explain why the intermediate closure of GluN1-LBD is only seen close to helixes F and G in D2, which is the area near IHB. Indeed, previously reported MD simulations have proposed the importance of the orientations of these helixes for the partial agonism of GluN1 (Dravid et al.

2010). The small forces from TMD directed on the LBD were mimicked in the SMD simulations that pulled the D2 while D1 was kept fixed. In these simulations, intermediate closure could be seen, and again the stage was relatively stable and energetically favourable.

6.2 Filamin A interaction with peptide-ligands

6.2.1 MM-GBSA is able to rank ligand-peptides according to their binding affinities

As the FLNa domains belonging to group 1 share a similar binding groove, they are a good target for evaluating the capability of the MM-GBSA method to estimate ΔG_{bind} efficiently and reliably. There already exists reported experimental affinity data for the binding of GPIbα to various group 1 domains, as well as data of different ligands binding to FLNa21. Additionally, several crystal structures of these FLNa-peptide complexes are available, so plausible conformations for each peptide could be derived for the MD simulations and the following MM-GBSA calculations.

When the computational results were plotted against the reported experimental data, a high correlation was seen with every IGB-model studied for various ligands binding to FLNa21. Similarly, in the case of GPIbα binding to different FLNa domains, IGB1 and IGB2 correlated well with experimental data. However, in this case, IGB5 deviated from the other two models by showing a lower R^2. The explanation for this is likely the large fluctuation in energy levels with this IGB-model, which was visible when ΔG_{bind} was plotted against simulation time for each individual run. Accordingly, this led to a large standard deviation in the average ΔG_{bind} calculations. These observations emphasise the importance of extracting a sufficiently large number of snapshots for the MD-based free energy calculations. The large variation in results depending on the IGB-model selected also suggests that not all of them are suitable for protein-peptide interaction evaluation, at least in the case of filamins.

In general, the ΔG_{bind} of individual repeats converged well (III, Fig. S2). However, this did not occur invariably for every protein-ligand complex. This is natural for all MD simulations of proteins, as it has been shown that the equilibration of proteins in MD simulations is practically unfeasible (Genheden & Ryde 2012). Consequently, it is proposed that in place of one long simulation, several short runs should be considered for MM-GBSA based energy calculations (Genheden & Ryde 2010, 2012). For FLNa-peptide complexes, three repeats were used to calculate the average ΔG_{bind}, which smoothed the possible fluctuations of the individual runs.

6.2.2 SMD confirms the critical interactions between FLNa and bound peptide

Based on the experimentally solved FLNa-peptide complex structures, it is presumed that one particular serine residue plays a crucial role in the interaction between FLNa and its binding partners. This serine is highly conserved among the peptides that bind to the CD-face of FLNa domains (Razinia et al. 2012). The side-chain of the serine is able to hydrogen bond to a residue from the D-strand of the FLNa domain, in contrast to the mostly hydrophobic interactions prevailing on that side of the peptide (Kiema et al. 2006, Nakamura et al. 2006, Lad et al. 2008, Takala et al. 2008). For example, in the FLNa21-migfilin complex, mutation of this serine inhibited the migfilin binding, thus emphasising its important role (Lad et al. 2008). In addition, the serine is a potential site of phosphorylation in the integrins (Fagerholm et al. 2004), further underlining its importance for FLNa interactions. The critical role of this residue was seen in the SMD simulations, for which the H-bond involving the side-chain of the serine in position 4 of all the peptides was always the last to break. In the SMD simulations, force was applied evenly to each residue of the bound peptide. This may not represent the actual disengagement taking place *in vivo.* However, as seen in case of the serine side-chain, these simulations allow atom-level analysis of the key interactions between FLNa and the peptide-ligand.

6.3 TCPTP activation by small molecules

A putative binding site for mitoxantrone was identified near the N-terminus of TCPTP with both computational and experimental methods. As this site is surrounded by several glutamate residues, it would also enable the binding of positively charged α1-cyt. It has been previously shown that these activators compete for TCPTP binding in a concentration dependent manner (Mattila et al. 2010). In line with this, mutagenesis of the surface glutamates led to reduced binding of both mitoxantrone and α1-cyt, thus supporting the view for this site serving as the binding site for both activators. However, a known TCPTP agonist spermidine did not show binding to the TC37, suggesting a different mechanism of activation for this molecule.

It is known from a previous study that unlike TC45, the truncated TC37 form cannot be activated by α1-cyt (Mattila et al. 2005). This finding, together with the suggested shared binding site near the N-terminus, has allowed for the speculation of the TC45 C-terminal folding. A plausible hypothesis is that the non-catalytic C-terminal part of TC45 first covers the catalytic site of the TCPTP and then stabilises the protein by binding over the activator binding site (IV, Fig. S4). Binding activator molecules, for example mitoxantrone, release the C-terminal and expose the catalytic site. This way, the auto-inhibition of the enzyme would be precluded. The finding that glutamate mutations inhibit α1-cyt activation supports the view that C-terminal replacement by a bound activator is needed for the release of the auto-inhibition. In shorter TC37, the catalytic site would be covered, but the amino acid chain would be too short to fold over the activator binding site. Thus, activator binding does not lead to activation of the enzyme. This view is supported by earlier finding that TC37 cannot be activated by α1-cyt (Mattila et al. 2005).

Experimental results with DSF and phosphatase assay show that 1,2-diaminoanthraquinone is able to bind but not activate TCPTP. This molecule has similar core structure to that of mitoxantrone but lacks the flexible arms. Accordingly, it is likely that the hydrophilic arms are necessary for TCPTP activators to break the intramolecular bonds between the activator binding site and the C-terminal chain. This structural information, together with the identified binding site, may help in the development of novel TCPTP activators in future.

7 CONCLUSIONS

The main findings of the thesis, obtained by computational and experimental methods, are:

1. One particular interdomain hydrogen bond was shown to indicate the partial agonism of iGluRs. This H-bond is located between the D1 and D2 of LBD, and was frequently broken by partial agonists in MD simulations. According to the simulations, this bond could be used to distinguish partial agonists of at least GluN1 and GluA2 iGluR subtypes. MD simulations showed that partial agonists of iGluRs do not necessarily prevent full closure of the LBD. Instead, partial agonists are able to destabilise the closure.

2. The intermediate closure stage for partial agonist-bound GluN1-LBD was identified for the first time. This closure stage, unseen in any crystal structures, was reached both in free and constrained MD simulations with several partial agonists. MM-GBSA calculations showed that this stage is an energetically stable conformation, but does not exist at every part of the binding cavity. Three distinct closure stages are clearly visible at the area near helixes F and G where IHB is located. This part of the D2 is closely connected to TMD via a short linker, suggesting that forces from the TMD directed to LBD affect the conformation of this area. SMD simulations simulating these intramolecular forces were shown to recreate the same intermediate closure stage for GluN1-LBD with bound partial agonists.

3. MM-GBSA calculations for free energy of the binding of various peptides bound to FLNa domains were shown to correlate well with the experimental data. This computational approach could reliably rank both the binding of one ligand to all of the studied FLNa domains, as well as the binding of all used ligands to FLNa domain 21. Even though correlations in general were high regardless of the IGB

model used, large fluctuations seen in ΔG_{bind} values with IGB5 suggest that not all IGB models may be suitable for protein-peptide calculations of this nature. SMD simulations of FLNa-peptide complexes emphasised the critical role of one particular serine for the FLNa-peptide interaction. Thus, SMD simulations enable the atom-level analysis of the key interactions between FLNa and its binding partners.

4. Binding site for TCPTP activator mitoxantrone was identified near the N-terminus of the phosphatase. Both computational and experimental methods suggested that this site also serves as the binding site for α1-cyt, which competes with mitoxantrone for binding. However, a known TCPTP activator spermidine was shown to be unable to bind this site. A new mitoxantrone-like molecule was shown to bind TCPTP but not activate it. From these results, structural information could be derived that may be helpful in the development of new efficient activators for TCPTP, a promising target for tumor suppression.

Acknowledgements

This work was carried out during 2009–2013 at the University of Jyväskylä, at the Department of Biological and Environmental Science. The thesis work was funded by ISB - National Doctoral Programme in Informational and Structural Biology. The computational resources were provided by CSC - IT Center for Science.

I especially want to thank my supervisor Dr. Olli Pentikäinen for the invaluable advice and guidance during the thesis work. It has always been easy for me to work with you. You seem to be a mine of information regarding our field. Thank you for including me in your research group and not firing me even though you hardly ever beat me in frisbee golf.

I acknowledge the reviewers Dr. Geoffrey Swanson and Dr. Mikael Peräkylä for their constructive feedback. I am also very pleased that Dr. Phil Biggin accepted the invitation to act as the opponent of my dissertation. My thesis committee members Prof. Mark Johnson and Dr. Jarmo Käpylä are greatly acknowledged. I am also grateful for Dr. Ulla Pentikäinen for all the help with my research. Many thanks to Arja Mansikkaviita for good advice she gave me in the lab. Marko Havu is thanked for his help in proof-reading. I would also like to warmly thank all the collaborators and co-authors.

Many thanks to the present and former members of the CBL-group: Pekka Postila, Elisa Nurminen, Jarkko Koivunen, Salla Virtanen, Sanna Niinivehmas, and Jason Ahokas. Thank you Jenni and Paula for the BIT years and all our refreshing coffee breaks. I also want to thank all the SMB juniors at B- and C-corridors for the fun moments at work and at playing Kimble (and other challenging games). Similarly, many thanks to all my ISB friends for the unforgettable winter and spring meetings. Thanks also to all my friends outside the work.

I want to express my gratitude to my parents and my brother Teemu for their support and encouragement throughout my life. We have had both good and sad moments during the past years but we always hold together. Finally, I want to express my warmest gratitude to my lovely wife Maija and my always so cheerful firstborn Aapo. Maija, thank you for your endless love, help, and support.

YHTEENVETO (RÉSUMÉ IN FINNISH)

Ligandin sitoutumisen vaikutus proteiinin toimintaan

Proteiinit ovat välttämättömiä elintoiminnoillemme, koska ne vastaavat lähes kaikista solujen tehtävistä. Nämä aminohappoketjuista muodostuvat orgaaniset yhdisteet toimivat muassa solujen tukirakenteina, hormoneina, solukalvojen reseptoreina sekä aineenvaihdunnassa entsyymeinä. Proteiinien toiminta riippuu usein niiden vuorovaikutuksesta ligandien kanssa, ja ligandin sitoutumisella voikin olla suuri vaikutus proteiinin aktiivisuuteen ja rakenteeseen. Erityisen tärkeää tässä molekyylien välisessä vuorovaikutuksessa on spesifisyys – usein vain juuri oikean kokoinen ja muotoinen sekä varaukseltaan sopiva ligandi pystyy sitoutumaan proteiiniin ja saamaan aikaan muutoksia sen rakenteessa tai toiminnassa. Tämä spesifinen tunnistus on perustana myös nykyaikaiselle lääkekehitykselle, jossa proteiinien ja ligandien rakenteen ja toiminnan tuntemus mahdollistaa uusien lääkkeiden kehitystyön.

Tämä väitöskirja koostuu kolmesta osaprojektista, joita yhdistää proteiini-ligandi-vuorovaikutukset ja niiden merkitys proteiinien toiminnalle. Samoin kaikkia tämän väitöskirjan tutkimuksia yhdistää modernien laskennallisten menetelmien käyttö. Viime vuosien nopea tietokoneiden kehitys on mahdollistanut entistä tarkemmat ja luotettavammat laskennalliset tutkimukset. Yhdistettynä monipuolisiin kokeellisiin tutkimusmenetelmiin laskennalliset menetelmät voivat auttaa rakentamaan kattavan kuvan proteiinien ja ligandien välisistä vuorovaikutuksista atomitason tarkkuudella.

Väitöskirjan ensimmäisessä osaprojektissa tutkittiin ionotrooppisia glutamaattireseptoreja (iGluR). Nämä solukalvoreseptorit toimivat synapseissa ja osallistuvat hermoimpulssien välitykseen. Hermovälittäjäaine glutamaatin sitoutuessa reseptorin ligandinsitomisdomeeniin (LBD) rakenteelliset muutokset välittyvät solukalvolla olevaan, neljän reseptorialayksikön yhdessä muodostamaan ionikanavaan. Glutamaatti tai jokin muu niin sanottu täysi agonisti aiheuttaa iGluR-LBD:n kahden domeenin (D1 ja D2) vääntymisen kiinni, mikä johtaa ionikanavan hetkelliseen aukeamiseen ja ionien virtaamiseen solun sisälle. Solun sisään virranneet ionit muuttavat solun kalvopotentiaalia ja tuottavat hermoimpulssin, joka siirtyy eteenpäin hermosolussa. Täysien agonistien lisäksi tunnetaan partiaalisia agonisteja, jotka tuottavat osittaisen reseptorin aktivaation. Röntgenkristallografialla on osoitettu, että toisin kuin täydet agonistit, osittaiset eli partiaaliset agonistit sulkevat kainaatti- ja AMPA-tyypin iGluR-LBD:t vain osittain. NMDA-tyypin iGluR-LBD:n kohdalla ei ole aiemmin havaittu osittaista sulkeutumista, vaikka partiaalisten agonistien tiedetään tuottavan tässäkin reseptorityypissä vain epätäydellistä aktivaatiota.

Väitöskirjassa osoitetaan, että iGluR-LBD:n eräs D1- ja D2-domeenien välinen vetysidos on hyvä indikaattori partiaaliselle agonismille erityisesti AMPA- ja NMDA-reseptorien kohdalla. Tämä vetysidos katkesi toistuvasti molekyylidynamiikkasimulaatioissa, mikä viittaa siihen, että partiaaliset agonistit eivät välttämättä estä täysin iGluR-LBD:n sulkeutumista, vaan tekevät sulkeutumisen epästabiiliksi. Simulaatiotulosten perusteella domeenien välisen vetysidoksen tarkastelu mahdollistaa ainakin AMPA- ja NMDA-reseptorien kohdalla partiaalisten agonistien erottamisen täysistä agonisteista.

Saman osaprojektin seuraavassa vaiheessa keskityttiin NMDA-reseptoreihin ja niiden partiaalisen agonismin tutkimiseen. Työssä osoitettiin ensimmäistä kertaa NMDA-reseptorin LBD:llä osittainen sulkeutumisaste partiaalisen agonistin ollessa siihen sitoutuneena. Tämä osittain sulkeutunut rakenne havaittiin useilla partiaalisilla agonisteilla ja sekä vapaissa että ulkoista voimaa mallintavissa molekyylidynamiikkasimulaatioissa. Sitoutumisaffiniteetti proteiini–ligandi-kompleksille laskettiin molekyylidynamiikkasimulaatioihin pohjautuen MM-GBSA-menetelmällä. Tässä menetelmässä molekyylien sitoutumisaffiniteettia ennustetaan molekyylimekaniikan voimakenttien ja solvaatioenergian laskemisen avulla. Osittain sulkeutuneen LBD-rakenteen todettiin olevan energeettisesti vakaa, mutta se oli havaittavissa vain siinä osassa ligandin sitovaa taskua, joka on suoraan yhteydessä solukalvoa läpäisevään osaan reseptoria. Tämä viittaa siihen, että solukalvon läpäisevästä osasta LBD:iin kohdistuvat voimat vaikuttavat paikallisesti tämän domeenin osan konformaatioon. Väitöskirjan iGluR-LBD-osaprojektissa saadut tulokset voivat osaltaan auttaa reseptorityyppispesifien ligandien suunnittelussa esimerkiksi hermostollisten sairauksien hoitamiseksi.

Toisessa väitöskirjan osaprojekteista tutkittiin filamiini A:n (FLNa) ja siihen sitoutuvien peptidiligandien vuorovaikutusta ja sitoutumisaffiniteettia. FLNa:t sitovat ja stabiloivat aktiinia, tärkeää solun rakennetta tukevaa proteiinia. FLNa on pitkä homodimeeri, jonka molemmat monomeerit koostuvat aminoterminaalisesta osasta ja sitä seuraavista 24:stä immunoglubuliinin kaltaisesta domeenista. Aktiinin lisäksi FLNa:iden tiedetään sitovan lukuisia muita proteiineja, esimerkiksi solukalvon läpäiseviä proteiineja ja solun kiinnittymiseen ja liikkumiseen liittyviä proteiineja. Useat näistä sitoutuvat ylimääräisenä β-säikeenä FLNa-domeenien C- ja D-säikeiden väliin eli toimivat peptidiligandeina. Tiettyyn domeeniryhmään kuuluvilla tämä sitomiskohta on rakenteellisesti hyvin samankaltainen, ja samojen peptidiligandien tiedetäänkin pystyvän sitoutumaan useisiin FLNa-domeeneihin.

Väitöskirjassa tutkittiin mahdollisuutta käyttää laskennallisia menetelmiä FLNa:han kiinnittyvien peptidiligandien sitoutumisaffiniteetin luotettavaan arvioimiseen. Sitoutumisen vapaaenergia (G_{bind}) laskettiin MM-GBSA-menetelmällä MD-simulaatioihin pohjautuen useille eri FLNa-ligandi komplekseille. Saadut laskennalliset tulokset korreloivat hyvin aiemmissa tutkimuksissa saatujen kokeellisten tulosten kanssa riippumatta käytetystä mallista polaarisen solvataatioenergian laskemiseksi. MM-GBSA:n avulla voitiin luotettavasti arvioida sekä useiden eri ligandien sitoutumista yhteen FLNa-domeeniin että yhden ligandin sitoutumista useaan eri FLNa-domeeniin. Ulkoista voimaa mallintavilla MD-simulaatioilla osoitettiin, että kaikissa tutkituissa peptideissä oleva, samaan kohtaan FLNa-domeenia sitoutuva seriini on erityisen tärkeässä roolissa peptidiligandin kiinnittymisessä. Seriinin sivuketjun ja FLNa:n muodostama vetysidos katkesi jokaisessa FLNa–ligandi-kompleksissa viimeisenä peptidiä vedettäessä. Kaiken kaikkiaan tämä väitöskirjan osaprojekti osoitti, että laskennallisia menetelmiä voidaan luotettavasti käyttää ainakin filamiinien kohdalla proteiini–proteiini-vuorovaikutusten laskemiseen. Uusien FLNa:han sitoutuvien peptidiligandien etsiminen voi jatkossa helpottua MM-GBSA-menetelmää hyödyntämällä. On myös mahdollista suunnitella sitoutumisen kannalta optimaalisia peptidejä tällä menetelmällä.

Kolmannessa väitöskirjan osaprojektissa tutkittiin T-solun proteiinityrosiinifosfataasia (TCPTP) ja sen aktivointia pienmolekyyleillä. TCPTP on solunsisäinen fosfataasi, jota nimestään huolimatta tuotetaan kaikissa ihmiselimistön soluissa. TCPTP kykenee autoinhibitioon eli estämään oman entsyymiaktiivisuutensa C-terminaalisen ei-katalyyttisen osansa avulla. $\alpha1\beta1$-integriinin solun sisäinen osa pystyy palauttamaan aktiivisuuden. Tämän uskotaan tapahtuvan siten, että integriinipeptidi sitoutuu entsyymin N-terminaaliseen osaan ja syrjäyttää autoinhibition aiheuttavan C–terminaalisen osan. TCPTP säätelee negatiivisesti muun muassa useita syöpiin liittyviä reseptorityrosiinikinaaseja, joten spesifisten ja tehokkaiden aktivaattorimolekyylien kehittäminen voisi tuoda uusia mahdollisuuksia joidenkin syöpien hoitoon. Aiemmissa tutkimuksissa on löydetty kuusi TCPTP:tä aktivoivaa pienmolekyyliä, muun muassa mitoksantroni.

Väitöskirjassa pyrittiin selvittämään mitoksantronin sitoutumiskohta TCPTP:ssä. Lisäksi tutkittiin, mitkä rakenteelliset tekijät ovat tärkeitä aktivaattorimolekyyleille. Molekyylitelakoinnilla ja MD-simulaatioiden avulla löydettiin todennäköinen sitoutumispaikka mitoksantronille läheltä TCPTP:n N-terminaalia. Kokeelliset menetelmät ja oletetun sitoutumispaikan lähellä olevien aminohappojen mutatointi tukivat näkemystä sitoutumispaikan sijainnista ja sitä, että sama paikka toimii myös integriinipeptidin sitoutumiskohtana. Myös mitoksantronia rakenteellisesti muistuttavan 1,2-diaminoantrakinonin todettiin pystyvän sitoutumaan samaan paikkaan, mutta entsyymin aktivaatiota ei tämän molekyylin avulla tapahtunut. 1,2-diaminoantrakinonilta puuttuvat positiivisesti varautuneet joustavat käsivarsimaiset ulokkeet, jotka mitoksantronilla on. Tästä voitiin päätellä, että nämä varautuneet ulokkeet ovat todennäköisesti oleellinen piirre TCPTP-aktivaattoreissa entsyymin autoinhibition purkamiseksi. Tämä rakenteellinen informaatio yhdessä sitoutumispaikan tunnistamisen kanssa voi edistää uusien TCPTP:tä aktivoivien molekyylien kehittämistä.

REFERENCES

Aarsland, D., Ballard, C., Walker, Z., Bostrom, F., Alves, G., Kossakowski, K., Leroi, I., Pozo-Rodriguez, F., Minthon, L. & Londos, E. 2009. Memantine in patients with Parkinson's disease dementia or dementia with Lewy bodies: a double-blind, placebo-controlled, multicentre trial. *Lancet Neurol.* 8 (7), 613–618.

Ahmed, A. H., Wang, S., Chuang, H. H. & Oswald, R. E. 2011. Mechanism of AMPA receptor activation by partial agonists: disulfide trapping of closed lobe conformations. *J.Biol.Chem.* 286 (40), 35257–35266.

Ahmed, A. H., Ptak, C. P., Fenwick, M. K., Hsieh, C. L., Weiland, G. A. & Oswald, R. E. 2013. Dynamics of cleft closure of the GluA2 ligand-binding domain in the presence of full and partial agonists revealed by hydrogen-deuterium exchange. *J.Biol.Chem.* 288 (38), 27658–27666.

Alonso, A., Sasin, J., Bottini, N., Friedberg, I., Friedberg, I., Osterman, A., Godzik, A., Hunter, T., Dixon, J. & Mustelin, T. 2004. Protein tyrosine phosphatases in the human genome. *Cell* 117 (6), 699–711.

Alt, A., Weiss, B., Ogden, A. M., Li, X., Gleason, S. D., Calligaro, D. O., Bleakman, D. & Witkin, J. M. 2006. In vitro and in vivo studies in rats with LY293558 suggest AMPA/kainate receptor blockade as a novel potential mechanism for the therapeutic treatment of anxiety disorders. *Psychopharmacology (Berl)* 185 (2), 240–247.

Aoki, N. & Matsuda, T. 2002. A nuclear protein tyrosine phosphatase TC-PTP is a potential negative regulator of the PRL-mediated signaling pathway: dephosphorylation and deactivation of signal transducer and activator of transcription 5a and 5b by TC-PTP in nucleus. *Mol.Endocrinol.* 16 (1), 58–69.

Armstrong, N. & Gouaux, E. 2000. Mechanisms for activation and antagonism of an AMPA-sensitive glutamate receptor: crystal structures of the GluR2 ligand binding core. *Neuron* 28 (1), 165–181.

Armstrong, N., Sun, Y., Chen, G. Q. & Gouaux, E. 1998. Structure of a glutamate-receptor ligand-binding core in complex with kainate. *Nature* 395 (6705), 913–917.

Bayly, C. I., Cieplak, P., Cornell, W. & Kollman, P. A. 1993. A well-behaved electrostatic potential based method using charge restrains for deriving atomic charges: The RESP model. *J.Phys.Chem.* 97, 10269.

Berman, H. M., Westbrook, J., Feng, Z., Gilliland, G., Bhat, T. N., Weissig, H., Shindyalov, I. N. & Bourne, P. E. 2000. The Protein Data Bank. *Nucleic Acids Res.* 28 (1), 235–242.

Bourdeau, A., Dubé, N. & Tremblay, M. L. 2005. Cytoplasmic protein tyrosine phosphatases, regulation and function: the roles of PTP1B and TC-PTP. *Curr.Opin.Cell Biol.* 17 (2), 203–209.

Case, D. A., Darden, T. A., Cheatham, T., Babin,,C.L.Simmerling, J.Wang, R.E.Duke, R.Luo, M.Crowley, R.C.Walker, W.Zhang, K.M.Merz, B.Wang, S.Hayik, A.Roitberg, G.Seabra, I- Kolossváry, K.F.Wong, F.Paesani, J.Vanicek, X.Wu, S.R.Brozell, T.Steinbrecher, H.Gohlke, L.Yang, C.Tan, J.Mongan, V.Hornak, G.Cui, D.H.Mathews, M.G.Seetin, C.Sagui, V. & Kollman, P. A. 2008. Amber 10. *University of California, San Francisco*.

Chen, H. S., Kolahi, K. S. & Mofrad, M. R. 2009. Phosphorylation facilitates the integrin binding of filamin under force. *Biophys.J.* 97 (12), 3095–3104.

Chen, P. E., Geballe, M. T., Stansfeld, P. J., Johnston, A. R., Yuan, H., Jacob, A. L., Snyder, J. P., Traynelis, S. F. & Wyllie, D. J. 2005. Structural features of the glutamate binding site in recombinant NR1/NR2A N-methyl-D-aspartate receptors determined by site-directed mutagenesis and molecular modeling. *Mol.Pharmacol.* 67 (5), 1470–1484.

Chen, P. E., Geballe, M. T., Katz, E., Erreger, K., Livesey, M. R., O'Toole, K. K., Le, P., Lee, C. J., Snyder, J. P., Traynelis, S. F. & Wyllie, D. J. 2008. Modulation of glycine potency in rat recombinant NMDA receptors containing chimeric NR2A/2D subunits expressed in Xenopus laevis oocytes. *J.Physiol.* 586 (1), 227–245.

Citri, A. & Malenka, R. C. 2008. Synaptic plasticity: multiple forms, functions, and mechanisms. *Neuropsychopharmacology* 33 (1), 18–41.

Connolly, M. L. 1983. Analytical molecular surface calculation. *J.Appl.Cryst.* 16, 548–558.

Cool, D. E., Tonks, N. K., Charbonneau, H., Fischer, E. H. & Krebs, E. G. 1990. Expression of a human T-cell protein-tyrosine-phosphatase in baby hamster kidney cells. *Proc.Natl.Acad.Sci.U.S.A.* 87 (18), 7280–7284.

Cool, D. E., Tonks, N. K., Charbonneau, H., Walsh, K. A., Fischer, E. H. & Krebs, E. G. 1989. cDNA isolated from a human T-cell library encodes a member of the protein-tyrosine-phosphatase family. *Proc.Natl.Acad.Sci.U.S.A.* 86 (14), 5257–5261.

Darden, T.D.Y. & Pedersen, L. 1993. Particle mesh Ewald: An W Log(N) method for Ewald sums in large systems. *J.Chem.Phys.* 98, 10089–10092.

Dingledine, R., Borges, K., Bowie, D. & Traynelis, S. F. 1999. The glutamate receptor ion channels. *Pharmacol.Rev.* 51 (1), 7–61.

Dravid, S. M., Burger, P. B., Prakash, A., Geballe, M. T., Yadav, R., Le, P., Vellano, K., Snyder, J. P. & Traynelis, S. F. 2010. Structural determinants of D-cycloserine efficacy at the NR1/NR2C NMDA receptors. *J.Neurosci.* 30 (7), 2741–2754.

Egawa, T., Tsuneshige, A., Suematsu, M. & Yonetani, T. 2007. Method for determination of association and dissociation rate constants of reversible bimolecular reactions by isothermal titration calorimeters. *Anal.Chem.* 79 (7), 2972–2978.

Erreger, K., Geballe, M. T., Kristensen, A., Chen, P. E., Hansen, K. B., Lee, C. J., Yuan, H., Le, P., Lyuboslavsky, P. N., Micale, N., Jorgensen, L., Clausen, R. P., Wyllie, D. J., Snyder, J. P. & Traynelis, S. F. 2007. Subunit-specific agonist activity at NR2A-, NR2B-, NR2C-, and NR2D-containing N-methyl-D-aspartate glutamate receptors. *Mol.Pharmacol.* 72 (4), 907–920.

Fagerholm, S. C., Hilden, T. J. & Gahmberg, C. G. 2004. P marks the spot: site-specific integrin phosphorylation regulates molecular interactions. *Trends Biochem.Sci.* 29 (9), 504–512.

Feller, S. E., Zhang, Y. & Pastor, R. W. 1995. Constant pressure molecular dynamics simulation: The Langevin piston method. *J.Chem.Phys.* 103, 4613–4621.

Fogolari, F., Moroni, E., Wojciechowski, M., Baginski, M., Ragona, L. & Molinari, H. 2005. MM/PBSA analysis of molecular dynamics simulations of bovine beta-lactoglobulin: free energy gradients in conformational transitions? *Proteins* 59 (1), 91–103.

Fox, J. W., Lamperti, E. D., Eksioglu, Y. Z., Hong, S. E., Feng, Y., Graham, D. A., Scheffer, I. E., Dobyns, W. B., Hirsch, B. A., Radtke, R. A., Berkovic, S. F., Huttenlocher, P. R. & Walsh, C. A. 1998. Mutations in filamin 1 prevent migration of cerebral cortical neurons in human periventricular heterotopia. *Neuron* 21 (6), 1315–1325.

Frydenvang, K., Lash, L. L., Naur, P., Postila, P. A., Pickering, D. S., Smith, C. M., Gajhede, M., Sasaki, M., Sakai, R., Pentikainen, O.T., Swanson, G. T. & Kastrup, J. S. 2009. Full domain closure of the ligand-binding core of the ionotropic glutamate receptor iGluR5 induced by the high affinity agonist dysiherbaine and the functional antagonist 8,9-dideoxyneodysiherbaine. *J.Biol.Chem.* 284 (21), 14219–14229.

Furuike, S., Ito, T. & Yamazaki, M. 2001. Mechanical unfolding of single filamin A (ABP-280) molecules detected by atomic force microscopy. *FEBS Lett.* 498 (1), 72–75.

Furukawa, H. & Gouaux, E. 2003. Mechanisms of activation, inhibition and specificity: crystal structures of the NMDA receptor NR1 ligand-binding core. *EMBO J.* 22 (12), 2873–2885.

Furukawa, H., Singh, S. K., Mancusso, R. & Gouaux, E. 2005. Subunit arrangement and function in NMDA receptors. *Nature* 438 (7065), 185–192.

Galic, S., Klingler-Hoffmann, M., Fodero-Tavoletti, M., Puryer, M. A., Meng, T., Tonks, N. K. & Tiganis, T. 2003. Regulation of insulin receptor signaling by the protein tyrosine phosphatase TCPTP. *Mol.Cell.Biol.* 23 (6), 2096–2108.

Genheden, S. & Ryde, U. 2010. How to obtain statistically converged MM/GBSA results. *J Comput Chem* 31 (4), 837–846.

Genheden, S. & Ryde, U. 2012. Will molecular dynamics simulations of proteins ever reach equilibrium? *Phys Chem Chem Phys* 14, 8662–8677.

Gohlke, H. & Case, D. A. 2004. Converging free energy estimates: MM-PB(GB)SA studies on the protein-protein complex Ras-Raf. *J Comput Chem* 25 (2), 238–250.

Gorlin, J. B., Yamin, R., Egan, S., Stewart, M., Stossel, T. P., Kwiatkowski, D. J. & Hartwig, J. H. 1990. Human endothelial actin-binding protein (ABP-280, nonmuscle filamin): a molecular leaf spring. *J.Cell Biol.* 111 (3), 1089–1105.

Hansen, K. B., Yuan, H. & Traynelis, S. F. 2007. Structural aspects of AMPA receptor activation, desensitization and deactivation. *Curr.Opin.Neurobiol.* 17 (3), 281–288.

Hao, L., Tiganis, T., Tonks, N. K. & Charbonneau, H. 1997. The noncatalytic C-terminal segment of the T cell protein tyrosine phosphatase regulates activity via an intramolecular mechanism. *J.Biol.Chem.* 272 (46), 29322–29329.

Hawkins, G. D., Cramer, C. J. & Truhlar, D. G. 1996. Parametrized models of aqueous free energies of solvation based on pairwise descreening of solute atomic charges from a dielectric medium. 100, 19824–19839.

Heikkinen, O. K., Ruskamo, S., Konarev, P. V., Svergun, D. I., Iivanainen, T., Heikkinen, S. M., Permi, P., Koskela, H., Kilpeläinen, I. & Ylänne, J. 2009. Atomic structures of two novel immunoglobulin-like domain pairs in the actin cross-linking protein filamin. *J.Biol.Chem.* 284 (37), 25450–25458.

Hendriks, W. J., Elson, A., Harroch, S. & Stoker, A. W. 2008. Protein tyrosine phosphatases: functional inferences from mouse models and human diseases. *FEBS J.* 275 (5), 816–830.

Horning, M. S. & Mayer, M. L. 2004. Regulation of AMPA receptor gating by ligand binding core dimers. *Neuron* 41 (3), 379–388.

Hou, T., Wang, J., Li, Y. & Wang, W. 2011. Assessing the performance of the MM/PBSA and MM/GBSA methods. 1. The accuracy of binding free energy calculations based on molecular dynamics simulations. *J. Chem. Inf. Model* 51 (1), 69–82.

Inanobe, A., Furukawa, H. & Gouaux, E. 2005. Mechanism of partial agonist action at the NR1 subunit of NMDA receptors. *Neuron* 47 (1), 71–84.

Ithychanda, S. S. & Qin, J. 2011. Evidence for multisite ligand binding and stretching of filamin by integrin and migfilin. *Biochemistry* 50 (20), 4229–4231.

Ithychanda, S. S., Hsu, D., Li, H., Yan, L., Liu, D. D., Das, M., Plow, E. F. & Qin, J. 2009. Identification and characterization of multiple similar ligand-binding repeats in filamin: implication on filamin-mediated receptor clustering and cross-talk. *J.Biol.Chem.* 284 (50), 35113–35121.

Iversen, L. F., Moller, K. B., Pedersen, A. K., Peters, G. H., Petersen, A. S., Andersen, H. S., Branner, S., Mortensen, S. B. & Moller, N. P. H. 2002. Structure determination of T cell protein-tyrosine phosphatase. *J.Biol.Chem.* 277 (22), 19982–19990.

Jones, G., Willett, P. & Glen, R. C. 1995. A genetic algorithm for flexible molecular overlay and pharmacophore elucidation. *J.Comput.Aided Mol.Des.* 9 (6), 532–549.

Jones, G., Willett, P., Glen, R. C., Leach, A. R. & Taylor, R. 1997. Development and validation of a genetic algorithm for flexible docking. *J.Mol.Biol.* 267 (3), 727–748.

Kalia, L. V., Kalia, S. K. & Salter, M. W. 2008. NMDA receptors in clinical neurology: excitatory times ahead. *Lancet Neurol.* 7 (8), 742–755.

Kaye, S. L., Sansom, M. S. P. & Biggin, P. C. 2006. Molecular dynamics simulations of the ligand-binding domain of an N-methyl-D-aspartate receptor. *J.Biol.Chem.* 281 (18), 12736–12742.

Kiema, T., Lad, Y., Jiang, P., Oxley, C. L., Baldassarre, M., Wegener, K. L., Campbell, I. D., Ylänne, J. & Calderwood, D. A. 2006. The molecular basis of filamin binding to integrins and competition with talin. *Mol.Cell* 21 (3), 337–347.

Kinarsky, L., Feng, B., Skifter, D. A., Morley, R. M., Sherman, S., Jane, D. E. & Monaghan, D. T. 2005. Identification of subunit- and antagonist-specific amino acid residues in the N-Methyl-D-aspartate receptor glutamate-binding pocket. *J.Pharmacol.Exp.Ther.* 313 (3), 1066–1074.

Kraulis, P. 1991. MOLSCRIPT: A program to produce both detailed and schematic plots of protein structures. *J.Appl.Crystallogr.* 24, 946–950.

Kuusinen, A., Arvola, M. & Keinänen, K. 1995. Molecular dissection of the agonist binding site of an AMPA receptor. *EMBO J.* 14 (24), 6327–6332.

Lad, Y., Jiang, P., Ruskamo, S., Harburger, D. S., Ylänne, J., Campbell, I. D. & Calderwood, D. A. 2008. Structural basis of the migfilin-filamin interaction and competition with integrin beta tails. *J.Biol.Chem.* 283 (50), 35154–35163.

Lad, Y., Kiema, T., Jiang, P., Pentikäinen, O.T., Coles, C. H., Campbell, I. D., Calderwood, D. A. & Ylänne, J. 2007. Structure of three tandem filamin domains reveals auto-inhibition of ligand binding. *EMBO J.* 26 (17), 3993–4004.

Lam, M. H., Michell, B. J., Fodero-Tavoletti, M., Kemp, B. E., Tonks, N. K. & Tiganis, T. 2001. Cellular stress regulates the nucleocytoplasmic distribution of the protein-tyrosine phosphatase TCPTP. *J.Biol.Chem.* 276 (40), 37700–37707.

Laskowski, R. A., MacArthur, M. W., Moss, D. S. & Thornton, J. M. 1993. PROCHECK: a program to check the stereochemical quality of protein structures. *J. Appl. Cryst* 26, 283–291.

Lehtonen, J. V., Still, D., Rantanen, V., Ekholm, J., Björklund, D., Iftikhar, Z., Huhtala, M., Repo, S., Jussila, A., Jaakkola, J., Pentikäinen, O., Nyrönen, T., Salminen, T., Gyllenberg, M. & Johnson, M. S. 2004. BODIL: a molecular modeling environment for structure-function analysis and drug design. *J.Comput.Aided Mol.Des.* 18 (6), 401–419.

Lisman, J. E. & McIntyre, C. C. 2001. Synaptic plasticity: a molecular memory switch. *Curr.Biol.* 11 (19), R788–791.

Lorenzen, J. A., Dadabay, C. Y. & Fischer, E. H. 1995. COOH-terminal sequence motifs target the T cell protein tyrosine phosphatase to the ER and nucleus. *J.Cell Biol.* 131 (3), 631–643.

Lu, X., Chen, J., Sasmono, R. T., Hsi, E. D., Sarosiek, K. A., Tiganis, T. & Lossos, I. S. 2007a. T-cell protein tyrosine phosphatase, distinctively expressed in activated-B-cell-like diffuse large B-cell lymphomas, is the nuclear phosphatase of STAT6. *Mol.Cell.Biol.* 27 (6), 2166–2179.

Massova, I. & Kollman, P. A. 2000. Combined molecular mechanical and continuum solvent approach (mm-pbsa/gbsa) to predict ligand binding. 18, 113–135.

Mattila, E., Auvinen, K., Salmi, M. & Ivaska, J. 2008. The protein tyrosine phosphatase TCPTP controls VEGFR2 signalling. *J.Cell.Sci.* 121, 3570–3580.

Mattila, E., Pellinen, T., Nevo, J., Vuoriluoto, K., Arjonen, A. & Ivaska, J. 2005. Negative regulation of EGFR signalling through integrin-alpha1beta1-mediated activation of protein tyrosine phosphatase TCPTP. *Nat.Cell Biol.* 7 (1), 78–85.

Mattila, E., Marttila, H., Sahlberg, N., Kohonen, P., Tähtinen, S., Halonen, P., Perälä, M. & Ivaska, J. 2010. Inhibition of receptor tyrosine kinase signalling by small molecule agonist of T-cell protein tyrosine phosphatase. *BMC Cancer* 10, 7.

Mayer, M. L. 2005. Crystal structures of the GluR5 and GluR6 ligand binding cores: molecular mechanisms underlying kainate receptor selectivity. *Neuron* 45 (4), 539–552.

Mayer, M. L. 2006. Glutamate receptors at atomic resolution. *Nature* 440 (7083), 456–462.

Mayer, M. L. 2011. Emerging models of glutamate receptor ion channel structure and function. *Structure* 19 (10), 1370–1380.

Mayer, M. L., Westbrook, G. L. & Guthrie, P. B. 1984. Voltage-dependent block by Mg2+ of NMDA responses in spinal cord neurones. *Nature* 309 (5965), 261–263.

Merritt, E. A. & Bacon, D. J. 1997. Raster3D: photorealistic molecular graphics. *Methods Enzymol* 277, 505–524.

Monyer, H., Sprengel, R., Schoepfer, R., Herb, A., Higuchi, M., Lomeli, H., Burnashev, N., Sakmann, B. & Seeburg, P. H. 1992. Heteromeric NMDA receptors: molecular and functional distinction of subtypes. *Science* 256 (5060), 1217–1221.

Mosinger, B. J., Tillmann, U., Westphal, H. & Tremblay, M. L. 1992. Cloning and characterization of a mouse cDNA encoding a cytoplasmic protein-tyrosine-phosphatase. *Proc.Natl.Acad.Sci.U.S.A.* 89 (2), 499–503.

Muppirala, M., Gupta, V. & Swarup, G. 2013. Emerging role of tyrosine phosphatase, TCPTP, in the organelles of the early secretory pathway. *Biochim.Biophys.Acta* 1833 (5), 1125–1132.

Mustelin, T., Vang, T. & Bottini, N. 2005. Protein tyrosine phosphatases and the immune response. *Nat.Rev.Immunol.* 5 (1), 43–57.

Nakamura, F., Stossel, T. P. & Hartwig, J. H. 2011. The filamins: organizers of cell structure and function. *Cell Adh Migr* 5 (2), 160–169.

Nakamura, F., Osborn, T. M., Hartemink, C. A., Hartwig, J. H. & Stossel, T. P. 2007. Structural basis of filamin A functions. *J.Cell Biol.* 179 (5), 1011–1025.

Nakamura, F., Pudas, R., Heikkinen, O., Permi, P., Kilpeläinen, I., Munday, A. D., Hartwig, J. H., Stossel, T. P. & Ylänne, J. 2006. The structure of the GPIb-filamin A complex. *Blood* 107 (5), 1925–1932.

Nakazawa, K., Quirk, M. C., Chitwood, R. A., Watanabe, M., Yeckel, M. F., Sun, L. D., Kato, A., Carr, C. A., Johnston, D., Wilson, M. A. & Tonegawa, S. 2002. Requirement for hippocampal CA3 NMDA receptors in associative memory recall. *Science* 297 (5579), 211–218.

Nicoletti, F., Bockaert, J., Collingridge, G. L., Conn, P. J., Ferraguti, F., Schoepp, D. D., Wroblewski, J. T. & Pin, J. P. 2011. Metabotropic glutamate receptors: from the workbench to the bedside. *Neuropharmacology* 60 (7-8), 1017–1041.

Niinivehmas, S. P., Virtanen, S. I., Lehtonen, J. V., Postila, P. A. & Pentikäinen, O.T. 2011. Comparison of virtual high-throughput screening methods for the identification of phosphodiesterase-5 inhibitors. *J. Chem. Inf. Model* 51 (6), 1353–1363.

Nowak, L., Bregestovski, P., Ascher, P., Herbet, A. & Prochiantz, A. 1984. Magnesium gates glutamate-activated channels in mouse central neurones. *Nature* 307 (5950), 462–465.

Ogden, K. K. & Traynelis, S. F. 2011. New advances in NMDA receptor pharmacology. *Trends Pharmacol.Sci.* 32 (12), 726–733.

Onufriev, A., Bashford, D. & Case, D. A. 2004. Exploring protein native states and large-scale conformational changes with a modified generalized born model. *Proteins* 55 (2), 383–394.

Pantoliano, M. W., Petrella, E. C., Kwasnoski, J. D., Lobanov, V. S., Myslik, J., Graf, E., Carver, T., Asel, E., Springer, B. A., Lane, P. & Salemme, F. R. 2001. High-density miniaturized thermal shift assays as a general strategy for drug discovery. *J.Biomol.Screen.* 6 (6), 429–440.

Parnas, M., Katz, B., Lev, S., Tzarfaty, V., Dadon, D., Gordon-Shaag, A., Metzner, H., Yaka, R. & Minke, B. 2009. Membrane lipid modulations remove divalent open channel block from TRP-like and NMDA channels. *J.Neurosci.* 29 (8), 2371–2383.

Pentikainen, O. T., Settimo, L., Keinanen, K. & Johnson, M. S. 2003. Selective agonist binding of (S)-2-amino-3-(3-hydroxy-5-methyl-4-isoxazolyl)propionic acid (AMPA) and 2S-(2alpha,3beta,4beta)-2-carboxy-4-(1-methylethenyl)-3-pyrrolidineacetic acid (kainate) receptors: a molecular modeling study. *Biochem.Pharmacol.* 66 (12), 2413–2425.

Pentikäinen, U. & Ylänne, J. 2009. The regulation mechanism for the auto-inhibition of binding of human filamin A to integrin. *J.Mol.Biol.* 393 (3), 644–657.

Pentikäinen, U., Settimo, L., Johnson, M. S. & Pentikäinen, O.T. 2006. Subtype selectivity and flexibility of ionotropic glutamate receptors upon antagonist ligand binding. *Org. Biomol. Chem.* 4 (6), 1058–1070.

Pentikainen, U., Jiang, P., Takala, H., Ruskamo, S., Campbell, I. D. & Ylanne, J. 2011. Assembly of a filamin four-domain fragment and the influence of splicing variant-1 on the structure. *J.Biol.Chem.* 286 (30), 26921–26930.

Persson, C., Sävenhed, C., Bourdeau, A., Tremblay, M. L., Markova, B., Böhmer, F.,D., Haj, F. G., Neel, B. G., Elson, A., Heldin, C., Rönnstrand, L., Ostman, A. & Hellberg, C. 2004. Site-selective regulation of platelet-derived growth factor beta receptor tyrosine phosphorylation by T-cell protein tyrosine phosphatase. *Mol.Cell.Biol.* 24 (5), 2190–2201.

Petrey, D., Xiang, Z., Tang, C. L., Xie, L., Gimpelev, M., Mitros, T., Soto, C. S., Goldsmith-Fischman, S., Kernytsky, A., Schlessinger, A., Koh, I. Y. Y., Alexov, E. & Honig, B. 2003. Using multiple structure alignments, fast model building, and energetic analysis in fold recognition and homology modeling. *Proteins* 53 Suppl 6, 430–435.

Phillips, J. C., Braun, R., Wang, W., Gumbart, J., Tajkhorshid, E., Villa, E., Chipot, C., Skeel, R. D., Kalé, L. & Schulten, K. 2005. Scalable molecular dynamics with NAMD. *J. Comput. Chem.* 26 (16), 1781–1802.

Playford, M. P., Nurminen, E., Pentikainen, O. T., Milgram, S. L., Hartwig, J. H., Stossel, T. P. & Nakamura, F. 2010. Cystic fibrosis transmembrane conductance regulator interacts with multiple immunoglobulin domains of filamin A. *J.Biol.Chem.* 285 (22), 17156–17165.

Popowicz, G. M., Schleicher, M., Noegel, A. A. & Holak, T. A. 2006. Filamins: promiscuous organizers of the cytoskeleton. *Trends Biochem.Sci.* 31 (7), 411–419.

Postila, P. A., Swanson, G. T. & Pentikäinen, O.T. 2010. Exploring kainate receptor pharmacology using molecular dynamics simulations. *Neuropharmacology* 58 (2), 515–527.

Priestley, T., Marshall, G. R., Hill, R. G. & Kemp, J. A. 1998. L-687,414, a low efficacy NMDA receptor glycine site partial agonist in vitro, does not prevent hippocampal LTP in vivo at plasma levels known to be neuroprotective. *Br.J.Pharmacol.* 124 (8), 1767–1773.

Ramanoudjame, G., Du, M., Mankiewicz, K. A. & Jayaraman, V. 2006. Allosteric mechanism in AMPA receptors: a FRET-based investigation of conformational changes. *Proc.Natl.Acad.Sci.U.S.A.* 103 (27), 10473–10478.

Ramaswamy, S., Cooper, D., Poddar, N., MacLean, D. M., Rambhadran, A., Taylor, J. N., Uhm, H., Landes, C. F. & Jayaraman, V. 2012. Role of conformational dynamics in alpha-amino-3-hydroxy-5-methylisoxazole-4-propionic acid (AMPA) receptor partial agonism. *J.Biol.Chem.* 287 (52), 43557–43564.

Rastelli, G., Del Rio, A., Degliesposti, G. & Sgobba, M. 2010. Fast and accurate predictions of binding free energies using MM-PBSA and MM-GBSA. *J.Comput.Chem.* 31 (4), 797–810.

Razinia, Z., Makela, T., Ylanne, J. & Calderwood, D. A. 2012. Filamins in mechanosensing and signaling. *Annu.Rev.Biophys.* 41, 227–246.

Robertson, S. P. 2005. Filamin A: phenotypic diversity. *Curr.Opin.Genet.Dev.* 15 (3), 301–307.

Robertson, S. P., Twigg, S. R., Sutherland-Smith, A. J., Biancalana, V., Gorlin, R. J., Horn, D., Kenwrick, S. J., Kim, C. A., Morava, E., Newbury-Ecob, R., Orstavik, K. H., Quarrell, O. W., Schwartz, C. E., Shears, D. J., Suri, M., Kendrick-Jones, J., Wilkie, A. O. & OPD-spectrum Disorders Clinical Collaborative Group 2003. Localized mutations in the gene encoding the cytoskeletal protein filamin A cause diverse malformations in humans. *Nat.Genet.* 33 (4), 487–491.

Rognoni, L., Stigler, J., Pelz, B., Ylänne, J. & Rief, M. 2012. Dynamic force sensing of filamin revealed in single-molecule experiments. *Proc.Natl.Acad.Sci.U.S.A.* 109 (48), 19679–19684.

Ryckaert, J., Ciccotti, G. & Berendsen, H. J. 1977. Numerical Integration of the Cartesian Equations of motion of a system with constraints: Molecular dynamics of n-alkanes. *J.Comput.Phys.* 23, 327–341.

Sali, A. & Blundell, T. L. 1993. Comparative protein modelling by satisfaction of spatial restraints. *J.Mol.Biol.* 234 (3), 779–815.

Sang, C. N., Ramadan, N. M., Wallihan, R. G., Chappell, A. S., Freitag, F. G., Smith, T. R., Silberstein, S. D., Johnson, K. W., Phebus, L. A., Bleakman, D., Ornstein, P. L., Arnold, B., Tepper, S. J. & Vandenhende, F. 2004. LY293558, a novel AMPA/GluR5 antagonist, is efficacious and well-tolerated in acute migraine. *Cephalalgia* 24 (7), 596–602.

Sangwan, V., Paliouras, G. N., Abella, J. V., Dubé, N., Monast, A., Tremblay, M. L. & Park, M. 2008. Regulation of the Met receptor-tyrosine kinase by the protein-tyrosine phosphatase 1B and T-cell phosphatase. *J.Biol.Chem.* 283 (49), 34374–34383.

Schlick, T., Skeel, R.D., Brunger, A.T., Kale, L.V., Board, J.A., Hermans, J. & Schulten, K. 1999. Algorithmic Challenges in Computational Molecular Biophysics. *J.Comput.Phys.* 151, 9–48.

Schorge, S., Elenes, S. & Colquhoun, D. 2005. Maximum likelihood fitting of single channel NMDA activity with a mechanism composed of independent dimers of subunits. *J.Physiol.* 569 (Pt 2), 395–418.

Simoncic, P. D., Lee-Loy, A., Barber, D. L., Tremblay, M. L. & McGlade, C. J. 2002. The T cell protein tyrosine phosphatase is a negative regulator of janus family kinases 1 and 3. *Curr.Biol.* 12 (6), 446–453.

Simoncic, P. D., Bourdeau, A., Lee-Loy, A., Rohrschneider, L. R., Tremblay, M. L., Stanley, E. R. & McGlade, C. J. 2006. T-cell protein tyrosine phosphatase (Tcptp) is a negative regulator of colony-stimulating factor 1 signaling and macrophage differentiation. *Mol.Cell.Biol.* 26 (11), 4149–4160.

Sjoblom, T., Jones, S., Wood, L. D., Parsons, D. W., Lin, J., Barber, T. D., Mandelker, D., Leary, R. J., Ptak, J., Silliman, N., Szabo, S., Buckhaults, P., Farrell, C., Meeh, P., Markowitz, S. D., Willis, J., Dawson, D., Willson, J. K., Gazdar, A. F., Hartigan, J., Wu, L., Liu, C., Parmigiani, G., Park, B. H., Bachman, K. E., Papadopoulos, N., Vogelstein, B., Kinzler, K. W. & Velculescu, V. E. 2006. The consensus coding sequences of human breast and colorectal cancers. *Science* 314 (5797), 268–274.

Smith, L., Page, R. C., Xu, Z., Kohli, E., Litman, P., Nix, J. C., Ithychanda, S. S., Liu, J., Qin, J., Misra, S. & Liedtke, C. M. 2010. Biochemical basis of the interaction between cystic fibrosis transmembrane conductance regulator and immunoglobulin-like repeats of filamin. *J.Biol.Chem.* 285 (22), 17166–17176.

Sobolevsky, A. I., Rosconi, M. P. & Gouaux, E. 2009. X-ray structure, symmetry and mechanism of an AMPA-subtype glutamate receptor. *Nature* 462 (7274), 745–756.

Srinivasan, J., Miller, J., Kollman, P. A. & Case, D. A. 1998. Continuum solvent studies of the stability of RNA hairpin loops and helices. *J.Biomol.Struct.Dyn.* 16 (3), 671–682.

Stossel, T. P., Condeelis, J., Cooley, L., Hartwig, J. H., Noegel, A., Schleicher, M. & Shapiro, S. S. 2001. Filamins as integrators of cell mechanics and signalling. *Nature reviews.Molecular cell biology* 2 (2), 138–145.

Stuible, M., Doody, K. M. & Tremblay, M. L. 2008. PTP1B and TC-PTP: regulators of transformation and tumorigenesis. *Cancer Metastasis Rev.* 27 (2), 215–230.

Takala, H., Nurminen, E., Nurmi, S. M., Aatonen, M., Strandin, T., Takatalo, M., Kiema, T., Gahmberg, C. G., Ylänne, J. & Fagerholm, S. C. 2008. Beta2 integrin phosphorylation on Thr758 acts as a molecular switch to regulate 14-3-3 and filamin binding. *Blood* 112 (5), 1853–1862.

ten Hoeve, J., de Jesus Ibarra-Sanchez, M., Fu, Y., Zhu, W., Tremblay, M., David, M. & Shuai, K. 2002. Identification of a nuclear Stat1 protein tyrosine phosphatase. *Mol.Cell.Biol.* 22 (16), 5662–5668.

Tiganis, T., Bennett, A. M., Ravichandran, K. S. & Tonks, N. K. 1998. Epidermal growth factor receptor and the adaptor protein p52Shc are specific substrates of T-cell protein tyrosine phosphatase. *Mol.Cell.Biol.* 18 (3), 1622–1634.

Tomic, A., Gonzalez, M. & Tomic, S. 2012. The large scale conformational change of the human DPP III-substrate prefers the "closed" form. *J.Chem.Inf.Model.* 52 (6), 1583–1594.

Tonks, N. K. 2006. Protein tyrosine phosphatases: from genes, to function, to disease. *Nature reviews - Molecular cell biology* 7 (11), 833–846.

Tonks, N. K. 2013. Protein tyrosine phosphatases--from housekeeping enzymes to master regulators of signal transduction. *FEBS J.* 280 (2), 346–378.

Tonks, N. K. & Neel, B. G. 2001. Combinatorial control of the specificity of protein tyrosine phosphatases. *Curr.Opin.Cell Biol.* 13 (2), 182–195.

Traynelis, S. F., Wollmuth, L. P., McBain, C. J., Menniti, F. S., Vance, K. M., Ogden, K. K., Hansen, K. B., Yuan, H., Myers, S. J. & Dingledine, R. 2010. Glutamate receptor ion channels: structure, regulation, and function. *Pharmacol.Rev.* 62 (3), 405–496.

Tsui, V. & Case, D.A. 2001. Theory and applications of the generalized Born solvation model in macromolecular simulations. *Biopolymers* 56 (4), 275–291.

Unger, S., Mainberger, A., Spitz, C., Bahr, A., Zeschnigk, C., Zabel, B., Superti-Furga, A. & Morris-Rosendahl, D. J. 2007. Filamin A mutation is one cause of FG syndrome. *Am.J.Med.Genet.A.* 143A (16), 1876–1879.

UniProt Consortium 2013. Update on activities at the Universal Protein Resource (UniProt) in 2013. *Nucleic Acids Res.* 41 (Database issue), D43–47.

Urwyler, S., Floersheim, P., Roy, B. L. & Koller, M. 2009. Drug design, in vitro pharmacology, and structure-activity relationships of 3-acylamino-2-aminopropionic acid derivatives, a novel class of partial agonists at the glycine site on the N-methyl-D-aspartate (NMDA) receptor complex. *J.Med.Chem.* 52 (16), 5093–5107.

van der Flier, A. & Sonnenberg, A. 2001. Structural and functional aspects of filamins. *Biochim.Biophys.Acta* 1538 (2-3), 99–117.

Velazquez-Campoy, A., Ohtaka, H., Nezami, A., Muzammil, S. & Freire, E. 2004. Isothermal titration calorimetry. *Curr.Protoc.Cell.Biol.* Chapter 17, Unit 17.8.

Vicini, S., Wang, J. F., Li, J. H., Zhu, W. J., Wang, Y. H., Luo, J. H., Wolfe, B. B. & Grayson, D. R. 1998. Functional and pharmacological differences between recombinant N-methyl-D-aspartate receptors. *J.Neurophysiol.* 79 (2), 555–566.

Vijayan, R., Sahai, M. A., Czajkowski, T. & Biggin, P. C. 2010. A comparative analysis of the role of water in the binding pockets of ionotropic glutamate receptors. *Phys Chem Chem Phys* 12 (42), 14057–14066.

Wang, J., Wang, W., Kollman, P. A. & Case, D. A. 2006. Automatic atom type and bond type perception in molecular mechanical calculations. *J.Mol.Graph.Model.* 25 (2), 247–260.

Waxman, E. A. & Lynch, D. R. 2005. N-methyl-D-aspartate receptor subtypes: multiple roles in excitotoxicity and neurological disease. *Neuroscientist* 11 (1), 37–49.

Weston, M. C., Gertler, C., Mayer, M. L. & Rosenmund, C. 2006. Interdomain interactions in AMPA and kainate receptors regulate affinity for glutamate. *J.Neurosci.* 26 (29), 7650–7658.

Winblad, B., Jones, R. W., Wirth, Y., Stoffler, A. & Mobius, H. J. 2007. Memantine in moderate to severe Alzheimer's disease: a meta-analysis of randomised clinical trials. *Dement.Geriatr.Cogn.Disord.* 24 (1), 20–27.

Wood, P. L., Mahmood, S. A. & Moskal, J. R. 2008. Antinociceptive action of GLYX-13: an N-methyl-D-aspartate receptor glycine site partial agonist. *Neuroreport* 19 (10), 1059–1061.

Wyllie, D. J., Behe, P. & Colquhoun, D. 1998. Single-channel activations and concentration jumps: comparison of recombinant NR1a/NR2A and NR1a/NR2D NMDA receptors. *J.Physiol.* 510 (Pt 1) (Pt 1), 1–18.

Yamamoto, T., Sekine, Y., Kashima, K., Kubota, A., Sato, N., Aoki, N. & Matsuda, T. 2002. The nuclear isoform of protein-tyrosine phosphatase TC-PTP regulates interleukin-6-mediated signaling pathway through STAT3 dephosphorylation. *Biochem.Biophys.Res.Commun.* 297 (4), 811–817.

Zuo, Z., Gandhi, N. S., Arndt, K. M. & Mancera, R. L. 2012. Free energy calculations of the interactions of c-Jun-based synthetic peptides with the c-Fos protein. *Biopolymers* 97 (11), 899–909.

ORIGINAL PAPERS

I

FULL AND PARTIAL AGONISM OF IONOTROPIC GLUTAMATE RECEPTORS INDICATED BY MOLECULAR DYNAMICS SIMULATIONS

by

Postila, P.A., Ylilauri, M. & Pentikäinen, O.T. 2011.

Journal of Chemical Information and Modeling 51, 1037–1047

Reprinted with kind permission of American Chemical Society.

II

STRUCTURAL MECHANISM OF N-METHYL-D-ASPARTATE RECEPTOR TYPE 1 PARTIAL AGONISM

by

Ylilauri, M. & Pentikäinen, O.T. 2012.

PLoS One 7(10), e47604

Structural Mechanism of *N*-Methyl-D-Aspartate Receptor Type 1 Partial Agonism

Mikko Ylilauri, Olli T. Pentikäinen*

Computational Bioscience Laboratory, Department of Biological and Environmental Science & Nanoscience Center, University of Jyväskylä, Jyväskylä, Finland

Abstract

N-methyl-D-aspartate (NMDA) receptors belong to a family of ionotropic glutamate receptors that contribute to the signal transmission in the central nervous system. NMDA receptors are heterotetramers that usually consist of two GluN1 and GluN2 monomers. The extracellular ligand-binding domain (LBD) of a monomer is comprised of discontinuous segments that form the functional domains D1 and D2. While the binding of a full agonist glycine to LBD of GluN1 is linked to cleft closure and subsequent ion-channel opening, partial agonists are known to activate the receptor only sub-maximally. Although the crystal structures of the LBD of related GluA2 receptor explain the mechanism for the partial agonism, structures of GluN1-LBD cannot distinguish the difference between full and partial agonists. It is, however, probable that the partial agonists of GluN1 alter the structure of the LBD in order to result in a different pharmacological response than seen with full agonists. In this study, we used molecular dynamics simulations to reveal an intermediate closure-stage for GluN1, which is unseen in crystal structures. According to our calculations, this intermediate closure is not a transient stage but an energetically stable conformation. Our results demonstrate that the partial agonist cannot exert firm GluN1-LBD closure, especially if there is even a small force that disrupts the LBD closure. Accordingly, this result suggests the importance of forces from the ion channel for the relationship between pharmacological response and the structure of the LBD of members of this receptor family.

Citation: Ylilauri M, Pentikäinen OT (2012) Structural Mechanism of *N*-Methyl-D-Aspartate Receptor Type 1 Partial Agonism. PLoS ONE 7(10): e47604. doi:10.1371/journal.pone.0047604

Editor: Andrew Jenkins, Emory University, United States of America

Received May 17, 2012; **Accepted** September 12, 2012; **Published** October 15, 2012

Copyright: © 2012 Ylilauri, Pentikäinen. This is an open-access article distributed under the terms of the Creative Commons Attribution License, which permits unrestricted use, distribution, and reproduction in any medium, provided the original author and source are credited.

Funding: This study was funded by the National Doctoral Programme in Informational and Structural Biology (M.Y.). The funders had no role in study design, data collection and analysis, decision to publish, or preparation of the manuscript.

Competing Interests: The authors have declared that no competing interests exist.

* E-mail: olli.t.pentikainen@jyu.fi

Introduction

N-methyl-D-aspartate receptors (NMDARs) belong to a family of ionotropic glutamate receptors (iGluRs) that contribute to signal transmission in the central nervous system [1]. NMDARs play crucial roles in learning and synaptic plasticity, for example [2], [3], [4]. All the iGluRs have been implicated in various diseases, especially neurological disorders. Disease states linked to NMDARs include Parkinson's disease, schizophrenia and stroke, among others [5], [6]. Similar to GluA2 (Fig. 1A), NMDAR probably is a heterotetramer that usually consists of two GluN1 (NMDA-R1) and GluN2 (NMDA-R2) monomers [7]. The functional heterogeneity of NMDARs arises from a wide variety of GluN2 subunits (for a recent review, see [8]). The ligand-binding domain (LBD) of iGluRs is comprised of discontinuous segments that form the functional domains 1 and 2 (D1 and D2) [9]. Although the recombinant LBD forms only part of the iGluR monomer, it shows a similar ligand-binding affinity to that of wild-type receptors [10], [11], [12]. Thus, this domain has been widely applied in crystallography, for example [11], [12], [13], [14], [15], [16] (Fig. 1B–C). Full agonists provoke full LBD closure, leading to opening of the ion channel [13]. In contrast to the AMPA-selective glutamate receptor 2 (GluA2; GluR2) where partial agonists wedge the LBD into a moderately closed state [13], [17] (Fig. 1B), the crystal structures of GluN1 imply that the partial agonists induce full receptor closure [11] (Fig. 1C), pointing to a different mechanism. This view was supported by a recent study [18] that used luminescence resonance energy transfer (LRET) to measure the extent of cleft closure in GluN1. No difference was found between the closure stages of full or partial agonist bound GluN1-LBD. Interestingly, however, in the same study, GluN2-LBD exhibited an intermediate cleft closure when bound to a partial agonist.

In addition to many crystallization studies, the ligand binding and closure of the iGluR-LBD have been explored using various experimental methods, including electrophysiology [12], [19], [20], fluorescence resonance energy transfer [21], and radioligand binding [16]. In addition to these experimental approaches, several recent studies have also exploited sophisticated computational methods to examine the structure and function of iGluRs. In particular, molecular dynamics (MD) simulations have been utilized to study the motion of receptor and ligand-receptor interactions occurring in solvent [22], [23]. For example, the role of water molecules inside the ligand-binding cleft [24], the pharmacology of novel ligands [25], and the subtype selectivity of antagonist ligands [26] have been studied with the help of this *in silico* method. However, closing an open-cleft receptor with a bound ligand has been reached computationally thus far only when exploited with biased MD simulations, for example the umbrella sampling method [27].

The antagonism of NMDA receptors has been widely studied for possible treatment of many neurological disorders [5], [28]. However, it has been proposed that partial agonists could be more

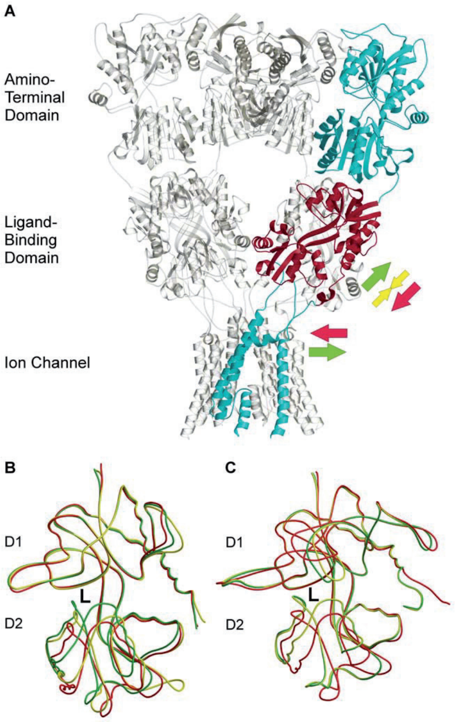

Figure 1. The crystal structure of iGluRs. (A) The crystal structure of GluA2 shows that it functions as a tetramer and (B) that the closure of the LBD determines the pharmacological behavior of GluA2. (C) On the contrary to GluA2, partial agonism of the NMDA receptors is ambiguous. In (A), one LBD (from PDB: 3KG2) is highlighted in red. The arrows depict the potential forces that occur during full agonist binding (green), partial agonist binding (yellow), and closure of the ion channel (red). In (B) and (C), superimposed structures with full agonist (green), partial agonist (yellow), and antagonist (red) are shown. Ligand binding site between domains D1 and D2 is depicted as letter L. Structures (PDB-codes) used are 3KG2 [7] in (A), 1FTJ, 1FTK, and 1FTL [13] in (B) and 1PB7, 1PB9, and 1Y1M [11], [12] in (C).
doi:10.1371/journal.pone.0047604.g001

advantageous as therapeutics because of their capability to permit some level of normal synaptic transmission while simultaneously suppressing excessive activation [29], [30], [31]. In fact, it has recently become evident that GluN1-specific partial agonists could be used to treat autism, for example (see [32] for review). However, although a growing number of studies concerning partial agonism of NMDA receptors have been published (see for example [12], [20], [33], [34]), only a few have examined the structure and motion of the LBD and its interactions with the ligand at the atomic level [22], [35], [36].

We have previously shown in MD simulations that the GluN1-LBD is able to adjust to more open conformations than crystallization studies have shown [36]. In addition, we have suggested that the stability of the cleft closure is associated with partial agonism. Incomplete closure of the GluN1-LBD with a bound partial agonist is not only interesting but also highly important pharmacologically. Indeed, it has been shown that the intrasubunit movements at linkers between LBD and transmembrane (TM) region are tightly coupled across the four subunits of NMDAR [37]. Thus, the binding of partial agonist molecules to two GluN1 subunits of the tetrameric receptor, which leads to incomplete closure of the LBD, would prevent full ion channel opening despite simultaneous full agonist binding to two GluN2 subunits.

In the present study, various computational methods were utilized in order to obtain a detailed view of the interactions taking place when a partial agonist binds in the GluN1-LBD. We performed steered molecular dynamics (SMD) simulations to study the firmness of full or partial agonist bound GluN1 structures. We also used constraint-free MD simulations to study the different closure stages and critical interactions of GluN1 with bound ligand. In addition, ligand-binding energetics with different closure stages of GluN1 were measured using the molecular mechanics generalized Born/surface area (MMGB/SA) method [38], [39].

Results and Discussion

We have previously shown that full agonists keep the iGluR-LBD closed, whereas partial agonists destabilize the cleft closure [36]. To examine LBD closure in detail, we measured the distances between various atoms from MD and SMD trajectories to investigate the interactions that take place between the ligand and GluN1 during the closure of the GluN1 ligand-binding cleft. In addition, visual inspection of the LBD in snapshot structures of MD aided the evaluation of changes in the conformations of amino acids participating in the ligand binding.

In constraint-free MD simulations, a full agonist, glycine, and partial agonists D-cycloserine, 1-aminocyclopropane-1-carboxylic acid (ACPC), and 1-aminocyclobutane-1-carboxylic acid (ACBC) were inserted into the open-cleft conformation of GluN1-LBD. In MD simulations, the smaller ligands glycine, D-cycloserine, and ACPC induced closure of the cleft (Figs. 2A–B and S1A), whereas ACBC, which has a bulkier structure, did not (Fig. S1B). Using glycine, this closure was sometimes obtained after 15 ns (Fig. 2B). However, in some simulations, closure occurred only after 120 ns. For D-cycloserine and ACPC, the closure times for GluN1-LBD were 19 ns and 6 ns, respectively (Figs. 2A and S1A). However, this result was not obtained regularly with either partial agonist in up to 127 ns simulations using the same setup. In this study, for the first time, the ligand-induced iGluR-LBD closure was repeatedly obtained in a constraint-free MD simulation with no artificial modifications (e.g., umbrella sampling, temperature shift, etc.). It is most likely that the closure of the GluN1 cleft is easier to obtain in a constraint-free MD simulation than closure of the other iGluRs because the solvent molecules are not as crucial in the ligand-binding process. The easier closure of GluN1 with bound agonist ligand is thus likely due to the lack of polar interactions between bound ligand and the D2, which is the case with other iGluR subtypes.

It is interesting to note that contrary to simulations with a full agonist, with all partial agonists a relatively stable intermediately closed conformation stage of the LBD appears to exist (Fig. 2C). In each partial agonist studied, this phase extended over a period of several nanoseconds, up to 16 ns in one of the MD simulations with D-cycloserine (Figs. 3A and S1). In the closed conformation, an interdomain hydrogen bond (IHB) exists between Gly485^{N}-Gln686^{O}. The IHB has previously been shown to be an efficient indicator of cleft closure [36]. However, in the intermediate closure, this distance is clearly longer (4-5 Å with D-cycloserine

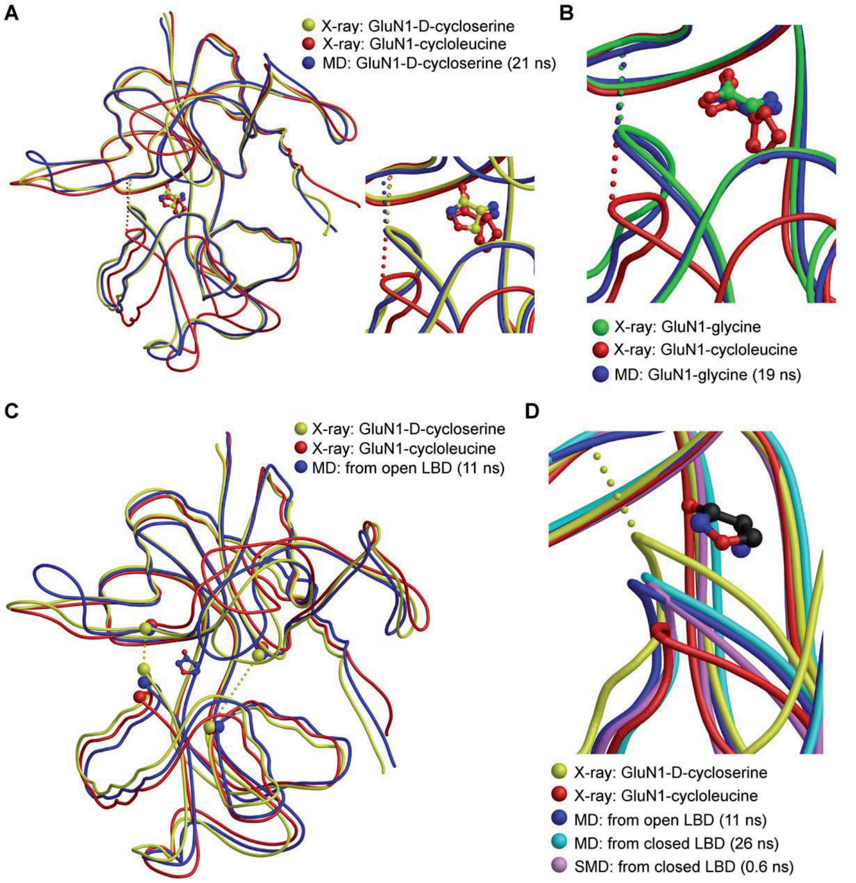
A
X-ray: GluN1-D-cycloserine
X-ray: GluN1-cycloleucine
MD: GluN1-D-cycloserine (21 ns)
B
X-ray: GluN1-glycine
X-ray: GluN1-cycloleucine
MD: GluN1-glycine (19 ns)
C
X-ray: GluN1-D-cycloserine
X-ray: GluN1-cycloleucine
MD: from open LBD (11 ns)
D
X-ray: GluN1-D-cycloserine
X-ray: GluN1-cycloleucine
MD: from open LBD (11 ns)
MD: from closed LBD (26 ns)
SMD: from closed LBD (0.6 ns)

Figure 2. MD and SMD simulations of ligand-bound GluN1-LBD. Free MD simulations indicate that (A) D-cycloserine and (B) glycine bound to open-cleft GluN1 (from PDB: 1Y1M) can close the LBD between D1 and D2, as seen in the crystal structures. (C) Contrary to crystal structures, a stable intermediate closure stage is seen in GluN1-LBD with bound partial agonists. Superimposition of a snapshot from a D-cycloserine simulation in Fig. 3A (blue line) with crystal structures of the same ligand (PDB: 1PB9) and antagonist ligand cycloleucine (from PDB: 1Y1M) is shown. Cα atoms of IHB residues (Gly485 and Gln686), as well as of residues Gln405 and Ala715, are depicted as CPK, and dotted lines represent the distances measured to study the closure of the cleft. (D) A close-up of the intermediately closed GluN1-D-cycloserine structures in free MD simulations – starting from both closed and open-cleft structures – as well as in SMD simulation starting from a closed-cleft structure (6 pN, blue line in Figure S2). Crystal structures of GluN1 with bound D-cycloserine (from PDB: 1PB9) and cycloleucine (from PDB: 1Y1M) are superimposed for comparison. Dotted lines in (A), (B), and (D) represent the IHB distance between Gly485^{N} and Gln686^{O}, which is an efficient indicator of cleft closure.
doi:10.1371/journal.pone.0047604.g002

and 5–6 Å with ACPC), albeit not as much as in the crystal structure of the GluN1-cycloleucine complex (7.1 Å). Interestingly, in this study, the intermediate closure obtained from an open-cleft conformation is very similar to that obtained from a closed-cleft conformation in the GluN1–D-cycloserine simulation (Fig. 3B) [36]. In addition to the intermediate closure with IHB distance of 4–5 Å, with ACBC, another intermediate stage was seen in some simulations at approximately 5.5 Å (Fig. S1B). The intermediate closure was not observed with full agonist glycine, regardless of the starting conformation (Fig. 3A–B). To investigate the effect of the observed intermediate closure on ligand positioning, we measured root-mean-square deviation (RMSD) values in the MD trajectories. According to average values calculated over intermediate and fully closed stages, RMSD for partial agonists remained stable. For example, in the D-cycloserine simulation of the open-cleft structure (Fig. 3A), an average value of RMSD (fit to previous frame) was 0.98±0.26 for both 3–18 and 20–30 ns time ranges. These results indicate that the closing of the open-cleft LBD does

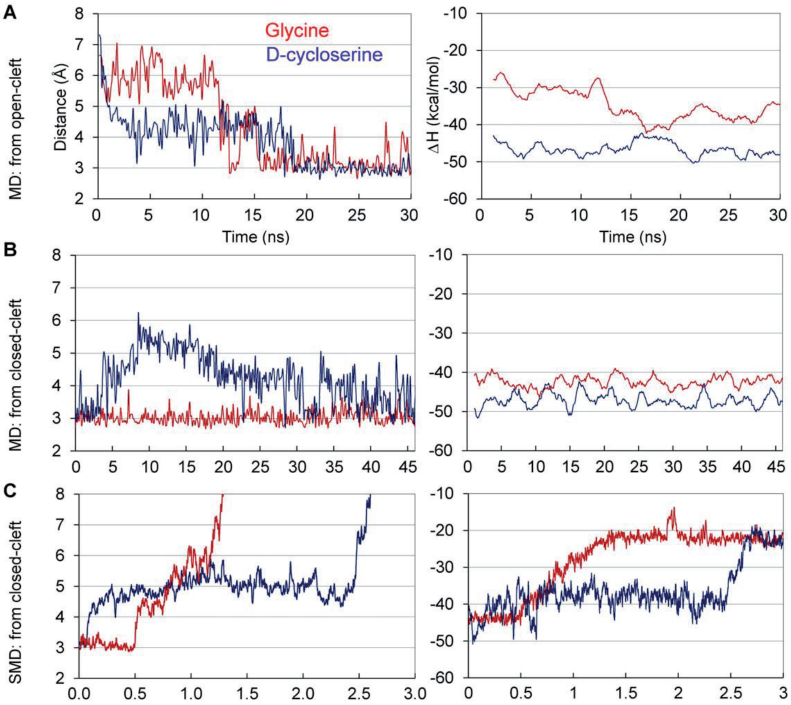

Figure 3. Relationship of GluN1-LBD closure and ΔH in ligand binding. Free MD simulations starting from (A) open and (B) closed LBD, and (C) SMD simulations (9 pN) from a closed LBD. The distances (left panel) are IHB distances (Gly485^{N}-Gln686^{O}). Corresponding binding enthalpies (ΔH) from the simulations are shown in the right panel. Results from all the SMD simulations performed are shown in Figure S2.
doi:10.1371/journal.pone.0047604.g003

not affect the fluctuation of the ligand conformation. However, in the open-cleft stage (0–3 ns), the average RMSD value was slightly higher (1.14±0.27), indicating that the ligand is more unrestrained to move in the cleft.

In addition to distances, we also studied the IHB angles of N-H-O and C-O-H in the MD simulation trajectories. IHB angles form between the main chain atom H (bonded to N) of Gly485 and O (bonded to C) of Gln686. Optimal angles for the triangles N-H-O and C-O-H are approximately 180° and 120°, respectively. The measured angles in both full agonist and partial agonist bound GluN1-LBD simulations deviated from these optimal values, yet they remained constant in the normal range. For D-cycloserine, the average angles of N-H-O and C-O-H when binding cavity was closed were 150±12 degrees and 155±12 degrees, respectively. For glycine, the same average angles were 148±12 for N-H-O and 161±10 for C-O-H. It must be noted that the corresponding angles in the crystal structures also differ somewhat from the optimal angle values: For glycine, the angles of N-H-O and C-O-H are 165.9 and 157.9, respectively. For D-cycloserine, the equivalent angles in an X-ray structure are 163.9 and 158.3.

To mimic the forces that likely apply to GluN1-LBD upon closure of the ion-channel (Figs. 1A and 4A: red arrows), we used SMD simulations with a constant force (6–10 pN) that was applied to C$^{\alpha}$ atoms of D2 while D1 was fixed. The direction of the force, which was defined by the vector that links the center of mass of C$^{\alpha}$ atoms of D1 and D2, simulated well the proposed force that was directed on the LBD and which induced the opening of the ligand-binding cleft (Fig. 4A, red arrows show the hypothetical movement of the ion channel forming transmembrane helix 3 (M3) that would lead into opening of the ion channel). These simulations revealed that the ligand-binding cleft closes more firmly with full agonists than partial agonists. In most cases, a glycine-bound structure remained closed even in a simulation with 8 pN force, although in some simulation runs the structure stayed shut at as high as 10 pN force. In contrast, the IHB in partial agonist simulations was broken readily with weaker forces, even at 6 pN (Fig. S2).

It is remarkable that in SMD simulations, with all the partial agonists the structures settled on the same intermediate closure as seen in free MD simulations (Figs. 3C and S2). In some of the 3 ns runs, when this closure stage was reached, it remained stable throughout the rest of the simulation. In some other runs, especially with higher forces, the LBD was first settled on the intermediate closure stage but later was fully opened. Similar to constraint-free MD simulations, this stage was not seen in any of the SMD runs with full agonist glycine-bound GluN1-LBD

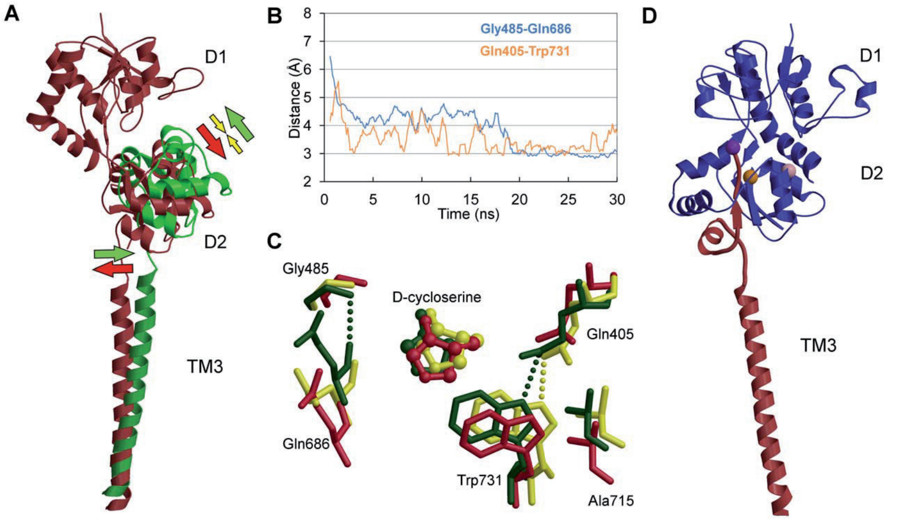

Figure 4. Closure mechanism of GluN1-LBD and connection to transmembrane domain. (A) Model showing the hypothesized conformational changes taking place at LBD and TM domain in binding of either an agonist or antagonist to cleft between D1 and D2. Agonist and antagonist bound models are colored green and red, respectively. Colored arrows depict the hypothesized forces affecting the conformation of the domains (full agonist in green, partial agonist in yellow and antagonist in red). (B) Distance measurements of Gly458^{N}-Gln686^{O} and Gln405^{OE1}-Trp731^{NE1} from D-cycloserine bound open-cleft GluN1-LBD taken from a constraint-free MD simulation trajectory. Comparison of the two distances reveals that there is a difference in the swiftness of closure of the LBD at various sides of the binding cleft. In addition, the intermediate closure is not seen ubiquitously at the binding cavity. In (C), superimposed structures are taken from the trajectory of the simulation in (B). The starting structure, cycloleucine-bound open-cleft GluN1 (PDB: 1Y1M), is colored red. Snapshots from intermediately closed (yellow) and fully closed (green) LBD are taken at time steps of 13 and 19 ns, respectively. In (D), part of an iGluR monomer (from GluA2 structure, PDB: 3KG2) show that the IHB is directly linked to M3. The purple ball represents the location of Gly458, which is the IHB-residue at D2 side of GluN1-LBD. Locations of Trp731 and Ala715 are depicted as orange and pink balls, respectively.
doi:10.1371/journal.pone.0047604.g004

(Figs. 3C and S2). The average IHB distances from SMD simulations were calculated for all the partial agonists studied at the intermediate closure stage. With bound D-cycloserine, GluN1-LBD settles to an average of 4.8±0.5 Å distance when intermediately closed. Similar closure degrees for ACPC and ACBC are 5.4±0.2 and 5.5±0.2 Å, respectively. It is difficult to extract definitive values due to the nature of the method and for the fact that the exact determination of the start and end points of the intermediate closure-stage is awkward. However, a rough comparison of the agonist efficacies of different ligands to experimental data ([12] [40]) suggests that the average closure degrees from MD simulations correlate with the experimental results: Priestley et al. (1995) [40] showed that D-cycloserine activates GluN1 by 88%±4 and ACBC by 33±7% compared to full agonist glycine, while Inanobe et al. (2005) [12] demonstrate ACPC and ACBC to have 80% and 42% activation, respectively. Thus, our results of distance calculations return, in some extent, these previous experimental findings; the smaller the IHB distance in intermediate closure, the more effective the ligand (Table 1).

The mechanism of closure of the LBD was analyzed in MD simulations starting from the open-cleft LBD. The distances of several atoms from MD trajectories were measured at different sides of the binding cavity. In addition, snapshots extracted from the trajectories were visually inspected. The distance measurements showed that closure does not occur similarly and simultaneously in every part of the cavity. This was most evident when the distance between Gln405 and Trp731 from D1 and D2, respectively, was compared to IHB-distance (Gly485-Gln686) in MD simulations with partial agonists (Figs. 4B and S3). These two

Table 1. Average IHB distance and ΔH from SMD simulations compared to experimentally obtained efficacies and EC_{50} values for various GluN1 agonists.

	Distance/Efficacy		**Energy/Potency**	
Ligand	**IHB (Å)**[a]	**Efficacy (%)**[b]	**ΔH (kcal/mol)**[c]	**EC_{50} (μM)**[d]
Glycine	2.9	100	−43.9	0.72
D-cycloserine	4.8	88	−38.4	8.2
ACPC	5.4	80	−43.9	0.65
ACBC	5.5	33	−38.7	6.6

[a] Calculated as average distances between Gly485^{N} and Gln686^{O} at the intermediate closure stage. For glycine, distance is measured from PDB-structure 1PB7.
[b] Experimental efficacies (from GluN1/GluN2B assemblies) compared to glycine. Data for D-cycloserine and ACBC from [40], ACPC from [12].
[c] Average ΔH calculated by MMGB/SA from the time-span of intermediate closure. For glycine, ΔH was averaged from the time period of fully closed state.
[d] EC_{50} data (from GluN1/GluN2B assemblies) obtained from literature: glycine and ACPC from [19], D-cycloserine and ACBC from [35] and [40], respectively.
doi:10.1371/journal.pone.0047604.t001

pairs are situated at separate sides of the cleft, IHB residing near helix F and loop 2 and Gln405-Trp731 between helices H and I. Although they both form a hydrogen bond as the binding cavity closes, Gln405-Trp731 bonding occurs much more rapidly. The swift closure at this part of the cavity is followed by a slower closure at the other end, which was seen in the IHB distance curve. A similar difference in the closure mechanism was previously seen in simulations of GluK1-LBD using partial agonist 9-deoxy-neoDH [23]. Interestingly, it appears that the intermediate closure stage has not been seen in the cleft area near helices H and I. In addition to the distance measurements, this is also evident when the superimposed snapshot structures are examined (Fig. 4C). Although an intermediate stage is clearly seen in residues forming the IHB, the area at the other side of the cavity has only two distinct closure stages. This might explain the previous results obtained with LRET, in which no intermediate closure of GluN1-LBD was seen with partial agonist when the distance was measured from Ala715 to Thr396 [18]. Because an isolated LBD was used in our MD studies, the N-terminal Thr396 is reasonably free to move during the simulations. Accordingly, it was not practical to measure this same distance in our study. However, Ala715, residing in helix H and depicted in Figure 4C, clearly shows movement similar to Trp731, which has only two distinct closure stages. The difference in the closure mechanism of LBD at separate sides of the cleft might be explained by taking into account how the LBD is linked to TM domain. M3, and especially the M3-S2 linker between TM and domain 2 of LBD, are presumed crucial in the gating process [7]. M3 helices form the ion pore in tetrameric iGluR [7], and M3-S2 likely transmits the conformational dynamics between TM and LBD. As shown in Figure 4D, the region of D2 near the IHB residues is closely linked to M3. Accordingly, any force directed on LBD from TM readily affects the conformation of this region of the LBD. On the contrary, Trp731 and Ala715 are not directly linked to TM (Fig. 4D). This possibly explains why the intermediate closure is seen only at some parts of the binding cleft. Additional explanation for the difference in the D1–D2 interaction at different parts of the cavity might be that while the IHB forms between main-chain atoms, the bond between Gln405 and Trp731 utilizes atoms of amino acid side-chains. Thus, the bond involving side chain atoms has more freedom to adapt to small movements at the D1–D2 interface compared to more restricted bond between main-chain N and O atoms. This difference between various parts of the cleft is analogous to that seen in the structure of GluA2 with bound kainate [9]. Earlier, it has been suggested that the movements at the hinge-region and the small movements of the Trp731 side-chain play a role in the mechanism of partial agonism [12]. However, our results indicate that there is no ligand-dependent motion at the hinge-region, and while the Trp731 indole ring may be able to slightly change its conformation depending on the ligand, the above mentioned hydrogen bond to Gln405 remains formed with both full and partial agonists. Thus, no intermediate closure is seen at that part of the ligand-binding cavity.

To study the energetic basis of the closure, ΔH was estimated from the MD and SMD trajectories by the MMGB/SA method. In the MD simulations of the open-cleft LBD with bound glycine, there was a clear decrease (10 kcal/mol) in energy when the cleft closed (Fig. 3A, 16 ns). In the simulations of the closed receptor, ΔH was similar throughout the simulation (Fig. 3B), indicating that the interactions in the GluN1-LBD complex did not change. In the SMD simulations, when the cleft opened, ΔH of glycine binding increased (Fig. 3C). Thus, MMGB/SA calculations indicated that the full agonist favors the closed LBD. In the MD simulation of open-stage GluN1-LBD with bound D-cycloserine, the ΔH was similar in both intermediate (Fig. 3A, 3–18 ns) and closed stages (Fig. 3A, 18–30 ns). This was more apparent in the MD simulation starting from the closed-stage LBD (Fig. 3B): the D-cycloserine-complex opened and remained at the intermediate closure before closing again at a later stage. However, the level of the ΔH did not shift substantially during these changes. In the SMD simulation, the ΔH increased slightly (3–5 kcal/mol) when the LBD opened to the intermediate closure (Fig. 3C). This increase could be explained by the fact that exerting a constant force to pull the D2 affects the binding conformation of D-cycloserine. With ACPC and ACBC, a similar trend was seen in SMD simulations: when the LBD opened to an intermediate stage, the ΔH typically increased only negligibly (Fig. S4). When the calculated ΔH values from SMD simulations (glycine: −43.9 kcal/mol; ACPC: −43.9 kcal/mol; D-cycloserine: −38.4 kcal/mol; ACBC: −38.7 kcal/mol), averaged for the time span of intermediate closure state (fully closed state for glycine), are compared to EC_{50} values reported for agonists (glycine: 0.72 μM [19]; ACPC: 0.85 μM [19]; D-cycloserine: 8.2 μM [35]; ACBC: 6.6 μM [40]), a good correlation can be seen (Table 1). To conclude, full closure of the GluN1-full agonist complex is clearly energetically preferred. On the contrary, with partial agonists the complete closure of GluN1-ligand complex is not necessarily energetically preferred, or at least, the difference between fully and partially closed stages is very small. According to our results from SMD with all three partial agonists, any stress on the LBD, such as from the ion-channel, can force the receptor cleft into the intermediate closure stage.

The co-crystal structures of GluN1-LBD with ligands, contrary to other iGluRs, imply that the degree of domain closure is similar with both full and partial agonists [11], [12]. In this study, we showed an intermediate closure stage exists for GluN1 with a bound partial agonist, similar to that reported for the GluA2-kainate complex [13]. This resemblance is apparent when the structures are superimposed (Figs. 2C–D and 4C). In addition to IHB-distance measurements (Fig. 3), the MMGB/SA calculations showed that this intermediate closure is not a transient stage but a stable and energetically favored conformation. As the agonist binds to the LBD, the ion channel opens. However, it also closes rapidly either by opening the LBD after releasing the bound agonist or, in the case of non-NMDA iGluRs, by entering the desensitization state. In other words, the ion channel persists in staying closed, and accordingly, based on our results it could be hypothesized that there is a force directed on the LBD that segregates D1 from D2. This force would transmit from M3 to LBD via the short linker and affects the conformation at the regions of D2 most closely linked to it. Such force from the TM would not be observed when only isolated LBDs are used, which would explain the missing intermediate closure from the crystal structures of partial agonist bound GluN1-LBD. Based on our results, partial agonists probably keep the receptor slightly open, as previously reported for other iGluR subtypes.

Methods

Starting structures

The complete structures of GluN1-LBD monomers with D-cycloserine (PDB: 1PB9) [11], ACPC (PDB: 1Y20) [12], ACBC (PDB: 1Y1Z) [12], glycine (PDB: 1PB7) [11], and cycloleucine (PDB: 1Y1M) [12] were built based on the alignment of the correspondent crystal structure and the rat sequence (GRIN1) [41] using MALIGN in BODIL [42] and NEST [43]. Note that monomer structure of GluN1 was used instead of GluN1/GluN2 dimer. This was done due to there are only D1–D1 interactions seen in the crystal structure of the GluN1-GluN2 LBD-dimer

(PDB: 2A5T) [15], and because there is as of yet no solved crystal structures of full tetrameric NMDA receptor; thus, it is currently not possible to confirm the actual interactions existing between GluN1 and GluN2.

For parameterization, the 3D structures of ligands were optimized quantum mechanically with GAUSSIAN03 (Gaussian, Inc., Wallingford, CT) at the HF/6-31+G* level using a polarizable continuum model. The RESP method [44] was used to calculate the atom-centered point charges from the electrostatic potentials. TLEAP in Antechamber-1.27 [45] was used to: (1) generate force field parameters; (2) add hydrogen atoms; (3) neutralize the system by adding two chloride ions; and (4) solvate the system with a rectangular box of transferable intermolecular potential three-point (TIP3P) water molecules extending 13 Å in every dimensions around the solute. The dimensions of the water-filled box in simulations starting from open and closed LBD were 86×87×97 Å and 94×86×91 Å, respectively. Number of water molecules in the box was approximately 20,900 in a box with the open-cleft GluN1-LBD and 17,800 with the closed-cleft.

Constraint-free MD simulations were performed for the open-cleft structure of GluN1-LBD, taken from the cycloleucine-bound complex (PDB: 1Y1M) [12]. The ligand position was decided based on the superimposition of C$^{\alpha}$ atoms of glycine or D-cycloserine LBD structures with the cycloleucine structure using VERTAA in BODIL [42]. The antagonist ligand was removed and replaced by either glycine or D-cycloserine from their corresponding X-ray structures. The energy minimization and MD simulations of 30–127 ns were performed with NAMD2.6 [46] using AMBER03 force field. The equilibration of the system was performed in three steps: (1) energy minimization of the water molecules, counter-ions and amino acid side-chains (15,000 steps), while the rest of the system was kept constrained at the same time by restraining C$^{\alpha}$ atoms with a harmonic force of 5 kcal mol^{-1} Å^{-2}; (2) energy minimization of the whole system without constrains (15,000 steps); and (3) MD simulation run with restrained C$^{\alpha}$ atoms in constant pressure (30,000 steps). Finally, unstrained production MD simulations were performed (30–127 ns). All production simulations were repeated three times. The temperature was kept at 300 K with Langevin dynamics for all non-hydrogen atoms, using a Langevin damping coefficient of 5 ps^{-1}. The pressure was kept at 1 atm with Nosé-Hoover Langevin piston [47] with an oscillation time scale of 200 fs and a damping time scale of 100 fs. An integration time step of 2 fs was used under a multiple time stepping scheme [48]. The bonded and short-range interactions were calculated every third step. A cutoff value of 12 Å was used for the short-range electrostatic interactions and van der Waals forces to smoothen the cutoff. The simulations were conducted under periodic boundary conditions, and the long-range electrostatics were counted with the particle mesh Ewald method [49]. The hydrogen bonds were restrained by the SHAKE algorithm [50].

In steered molecular dynamics (SMD) simulations, the C$^{\alpha}$ atoms of D1 of GluN1-LBD (Met394-Tyr535 and Gly757-Ser800) were kept fixed while an external force was applied to the center of mass of the C$^{\alpha}$ atoms of D2 (Gln536-Ser756). The direction of the constant force (6–10 pN) was defined by the vector that links the center of mass of C$^{\alpha}$ atoms of D1 and D2. The simulations were performed as with constraint-free simulations, except that the SMD production runs of 3 ns were performed only after 720 ps unrestrained MD simulation, and the time step used in SMD production simulations was 1 fs.

Trajectory analyses of MD and SMD simulations were done by extracting snapshots at 360 ps intervals with PTRAJ in ANTECHAMBER 1.27 [45]. Various atom distances and closure angles, at 120 ps intervals, were measured with PTRAJ from amino acid residues in the ligand-binding pocket. RMSD values, fit to previous frame, were extracted from trajectories to study the ligand-positioning. Visual inspection of snapshots was performed with BODIL. A cutoff value of 3.4 Å was used as the upper limit for a hydrogen bonding distance.

The binding enthalpies (ΔH) of ligands with implicit solvent model were calculated from the MD and SMD trajectories using molecular mechanics generalized Born/surface area (MMGB/SA) method [38], [39] implemented in Amber10 [51]. Changes in the enthalpy were calculated from snapshots taken from the MD complex trajectory at 120 ps intervals.

Figures were generated with BODIL v. 0.81 and MOLSCRIPT v. 2.1.2 [52], and rendered with RASTER3D v. 2.7C [53].

Modeling the hypothetical M3 helix movements upon agonist ligand binding (Fig. 4A) was made using the following strategy: (1) D1 domain of GluA2-L-glutamate complex (PDB: 1FTJ) was superimposed with the D1 of the full length GluA2 structure (PDB: 3KG2) (2) D2 of another copy of the full length GluA2 structure was superimposed with D2 of GluA2-L-glutamate complex used in the step (1); finally (3), the intracellular end of the M3 helix of the full length GluA2 structure from step (2) was superimposed (while extracellular end was left in the modeled position) with that of the full length GluA2 structure used in the step (1).

Supporting Information

Figure S1 Constraint-free MD simulations of ACPC and ACBC. Free MD simulations starting from open GluN1-LBD are shown for (A) ACPC and (B) ACBC. IHB distance (Gly458^{N}-Gln686^{O}) measurement for two representative repeats is shown for both partial agonists. Simulations with bound ACPC show closure of the LBD (dark blue) and the stable intermediate stage (light blue). In simulations with ACBC, two distinct intermediate stages can be seen: one at 4–5 Å (light blue) and another at 5–6 Å (dark blue, starting from approximately 20 ns).
(TIF)

Figure S2 GluN1-LBD opening in SMD simulations. Openings of glycine, D-cycloserine, ACPC and ACBC-bound closed GluN1-LBD in SMD simulations are shown for various external forces. In the simulations, a constant force (6–10 pN) was applied to C$^{\alpha}$ atoms of D2 (Gln536-Ser756) while the C$^{\alpha}$ atoms of D1 (Met394-Tyr535 and Gly757-Ser800) were kept fixed. Three repeats (colored blue, purple and red) are shown for each ligand and force used.
(TIF)

Figure S3 Closure mechanism of glycine and ACPC-bound GluN1-LBD. Distance measurements of Gly458^{N}-Gln686^{O} (blue) and Gln405^{OE1}-Trp731^{NE1} (orange) from (A) glycine and (B) ACPC-bound open-cleft GluN1-LBD are taken from constraint-free MD simulation trajectories. Similar distance measurements for D-cycloserine bound LBD are shown in Figure 4B.
(TIF)

Figure S4 Calculated binding enthalpies (ΔH) from SMD simulations of ACPC and ACBC-bound GluN1-LBD. Compared to D-cycloserine, a similar trend was seen in SMD simulations of (A) ACPC and (B) ACBC: when the LBD opened to an intermediate stage, the ΔH increased only negligibly. With ACPC, this is seen from 1.5 to 2.5 ns and with ACBC, from 1.0 to 1.8 ns. IHB distance is shown in blue and the ΔH, estimated by the MMGB/SA method, in black.
(TIF)

Author Contributions

Conceived and designed the experiments: MY OTP. Performed the experiments: MY. Analyzed the data: MY OTP. Wrote the paper: MY OTP.

References

1. Traynelis SF, Wollmuth LP, McBain CJ, Menniti FS, Vance KM, et al. (2010) Glutamate receptor ion channels: structure, regulation, and function. Pharmacol Rev 62: 405–496.
2. Lisman JE, McIntyre CC (2001) Synaptic plasticity: a molecular memory switch. Curr Biol 11: R788–91.
3. Nakazawa K, Quirk MC, Chitwood RA, Watanabe M, Yeckel MF, et al. (2002) Requirement for hippocampal CA3 NMDA receptors in associative memory recall. Science 297: 211–218.
4. Citri A, Malenka RC (2008) Synaptic plasticity: multiple forms, functions, and mechanisms. Neuropsychopharmacology 33: 18–41.
5. Kalia LV, Kalia SK, Salter MW (2008) NMDA receptors in clinical neurology: excitatory times ahead. Lancet Neurol 7: 742–755.
6. Waxman EA, Lynch DR (2005) N-methyl-D-aspartate receptor subtypes: multiple roles in excitotoxicity and neurological disease. Neuroscientist 11: 37–49.
7. Sobolevsky AI, Rosconi MP, Gouaux E (2009) X-ray structure, symmetry and mechanism of an AMPA-subtype glutamate receptor. Nature 462: 745–756.
8. Paoletti P (2011) Molecular basis of NMDA receptor functional diversity. Eur J Neurosci 33: 1351–1365.
9. Armstrong N, Sun Y, Chen GQ, Gouaux E (1998) Structure of a glutamate-receptor ligand-binding core in complex with kainate. Nature 395: 913–917.
10. Kuusinen A, Arvola M, Keinänen K (1995) Molecular dissection of the agonist binding site of an AMPA receptor. EMBO J 14: 6327–6332.
11. Furukawa H, Gouaux E (2003) Mechanisms of activation, inhibition and specificity: crystal structures of the NMDA receptor NR1 ligand-binding core. EMBO J 22: 2873–2885.
12. Inanobe A, Furukawa H, Gouaux E (2005) Mechanism of partial agonist action at the NR1 subunit of NMDA receptors. Neuron 47: 71–84.
13. Armstrong N, Gouaux E (2000) Mechanisms for activation and antagonism of an AMPA-sensitive glutamate receptor: crystal structures of the GluR2 ligand binding core. Neuron 28: 165–181.
14. Mayer ML (2005) Crystal structures of the GluR5 and GluR6 ligand binding cores: molecular mechanisms underlying kainate receptor selectivity. Neuron 45: 539–552.
15. Furukawa H, Singh SK, Mancusso R, Gouaux E (2005) Subunit arrangement and function in NMDA receptors. Nature 438: 185–192.
16. Frydenvang K, Lash LL, Naur P, Postila PA, Pickering DS, et al. (2009) Full domain closure of the ligand-binding core of the ionotropic glutamate receptor iGluR5 induced by the high affinity agonist dysiherbaine and the functional antagonist 8,9-dideoxyneodysiherbaine. J Biol Chem 284: 14219–14229.
17. Jin R, Banke TG, Mayer ML, Traynelis SF, Gouaux E (2003) Structural basis for partial agonist action at ionotropic glutamate receptors. Nat Neurosci 6: 803–810.
18. Rambhadran A, Gonzalez J, Jayaraman V (2011) Conformational changes at the agonist binding domain of the N-methyl-D-aspartic acid receptor. J Biol Chem 286: 16953–16957.
19. Chen PE, Geballe MT, Katz E, Erreger K, Livesey MR, et al. (2008) Modulation of glycine potency in rat recombinant NMDA receptors containing chimeric NR2A/2D subunits expressed in Xenopus laevis oocytes. J Physiol 586: 227–245.
20. Kussius CL, Popescu GK (2009) Kinetic basis of partial agonism at NMDA receptors. Nat Neurosci 12: 1114–1120.
21. Ramanoudjame G, Du M, Mankiewicz KA, Jayaraman V (2006) Allosteric mechanism in AMPA receptors: a FRET-based investigation of conformational changes. Proc Natl Acad Sci U S A 103: 10473–10478.
22. Kaye SL, Sansom MSP, Biggin PC (2006) Molecular dynamics simulations of the ligand-binding domain of an N-methyl-D-aspartate receptor. J Biol Chem 281: 12736–12742.
23. Postila PA, Swanson GT, Pentikäinen OT (2010) Exploring kainate receptor pharmacology using molecular dynamics simulations. Neuropharmacology 58: 515–527.
24. Vijayan R, Sahai MA, Czajkowski T, Biggin PC (2010) A comparative analysis of the role of water in the binding pockets of ionotropic glutamate receptors. Phys Chem Chem Phys 12: 14057–14066.
25. Lash-Van Wyhe LL, Postila PA, Tsubone K, Sasaki M, Pentikäinen OT, et al. (2010) Pharmacological activity of C10-substituted analogs of the high-affinity kainate receptor agonist dysiherbaine. Neuropharmacology 58: 640–649.
26. Pentikäinen U, Settimo L, Johnson MS, Pentikäinen OT (2006) Subtype selectivity and flexibility of ionotropic glutamate receptors upon antagonist ligand binding. Org Biomol Chem 4: 1058–1070.
27. Lau AY, Roux B (2007) The free energy landscapes governing conformational changes in a glutamate receptor ligand-binding domain. Structure 15: 1203–1214.
28. Ogden KK, Traynelis SF (2011) New advances in NMDA receptor pharmacology. Trends Pharmacol Sci 32: 726–733.
29. Priestley T, Marshall GR, Hill RG, Kemp JA (1998) L-687,414, a low efficacy NMDA receptor glycine site partial agonist in vitro, does not prevent hippocampal LTP in vivo at plasma levels known to be neuroprotective. Br J Pharmacol 124: 1767–1773.
30. Wood PL, Mahmood SA, Moskal JR (2008) Antinociceptive action of GLYX-13: an N-methyl-D-aspartate receptor glycine site partial agonist. Neuroreport 19: 1059–1061.
31. Urwyler S, Floersheim P, Roy BL, Koller M (2009) Drug design, in vitro pharmacology, and structure-activity relationships of 3-acylamino-2-aminopropionic acid derivatives, a novel class of partial agonists at the glycine site on the N-methyl-D-aspartate (NMDA) receptor complex. J Med Chem 52: 5093–5107.
32. Moskal JR, Burgdorf J, Kroes RA, Brudzynski SM, Panksepp J (2011) A novel NMDA receptor glycine-site partial agonist, GLYX-13, has therapeutic potential for the treatment of autism. Neurosci Biobehav Rev 35: 1982–1988.
33. Banke TG, Traynelis SF (2003) Activation of NR1/NR2B NMDA receptors. Nat Neurosci 6: 144–152.
34. Moretti L, Pentikäinen OT, Settimo L, Johnson MS (2004) Model structures of the N-methyl-D-aspartate receptor subunit NR1 explain the molecular recognition of agonist and antagonist ligands. J Struct Biol 145: 205–215.
35. Dravid SM, Burger PB, Prakash A, Geballe MT, Yadav R, et al. (2010) Structural determinants of D-cycloserine efficacy at the NR1/NR2C NMDA receptors. J Neurosci 30: 2741–2754.
36. Postila PA, Ylilauri M, Pentikainen OT (2011) Full and Partial Agonism of Ionotropic Glutamate Receptors Indicated by Molecular Dynamics Simulations. J Chem Inf Model 51: 1037–1047.
37. Talukder I, Wollmuth LP (2011) Local constraints in either the GluN1 or GluN2 subunit equally impair NMDA receptor pore opening. J Gen Physiol 138: 179–194.
38. Tsui V, Case DA (2000–2001) Theory and applications of the generalized Born solvation model in macromolecular simulations. Biopolymers 56: 275–291.
39. Kollman PA, Massova I, Reyes C, Kuhn B, Huo S, et al. (2000) Calculating structures and free energies of complex molecules: combining molecular mechanics and continuum models. Acc Chem Res 33: 889–897.
40. Priestley T, Laughton P, Myers J, Le Bourdellés B, Kerby J, et al. (1995) Pharmacological properties of recombinant human N-methyl-D-aspartate receptors comprising NR1a/NR2A and NR1a/NR2B subunit assemblies expressed in permanently transfected mouse fibroblast cells. Mol Pharmacol 48: 841–848.
41. Moriyoshi K, Masu M, Ishii T, Shigemoto R, Mizuno N, et al. (1991) Molecular cloning and characterization of the rat NMDA receptor. Nature 354: 31–37.
42. Lehtonen JV, Still D, Rantanen V, Ekholm J, Björklund D, et al. (2004) BODIL: a molecular modeling environment for structure-function analysis and drug design. J Comput Aided Mol Des 18: 401–419.
43. Petrey D, Xiang Z, Tang CL, Xie L, Gimpelev M, et al. (2003) Using multiple structure alignments, fast model building, and energetic analysis in fold recognition and homology modeling. Proteins 53 Suppl 6: 430–435.
44. Bayly CI, Cieplak P, Cornell WD, Kollman PA (1993) A well-behaved electrostatic potential based method using charge restrains for deriving atomic charges: The RESP model. J Phys Chem 97: 10269.
45. Wang H, Liu Y, Huai Q, Cai J, Zoraghi R, et al. (2006) Multiple conformations of phosphodiesterase-5: implications for enzyme function and drug development. J Biol Chem 281: 21469–21479.
46. Phillips JC, Braun R, Wang W, Gumbart J, Tajkhorshid E, et al. (2005) Scalable molecular dynamics with NAMD. J Comput Chem 26: 1781–1802.
47. Feller SE, Zhang Y, Pastor RW (1995) Constant pressure molecular dynamics simulation: The Langevin piston method. J Chem Phys 103: 4613–4621.
48. Schlick T, Skeel RD, Brunger AT, Kalé LV, Board JAJ, et al. (1999) Algorithmic Challenges in Computational Molecular Biophysics. J Comput Phys 151: 9–48.
49. Darden T, York D, Pedersen L (1993) Particle mesh Ewald: An W Log(N) method for Ewald sums in large systems. J Chem Phys 98: 10089–10092.
50. Ryckaert J, Ciccotti G, Berendsen HJ (1977) Numerical Integration of the Cartesian Equations of motion of a system with constraints: Molecular dynamics of n-alkanes. J Comput Phys 23: 327.
51. Case DA, Cheatham TE3, Darden T, Gohlke H, Luo R, et al. (2005) The Amber biomolecular simulation programs. J Comput Chem 26: 1668–1688.
52. Kraulis P (1991) MOLSCRIPT: A program to produce both detailed and schematic plots of protein structures. J Appl Crystallogr 24: 946–950.
53. Merritt EA, Bacon DJ (1997) Raster3D: photorealistic molecular graphics. Methods Enzymol 277: 505–524.

Supplementary material

Structural Mechanism of *N*-Methyl-D-Aspartate Receptor Type 1 Partial Agonism

Mikko Ylilauri, Olli T. Pentikäinen

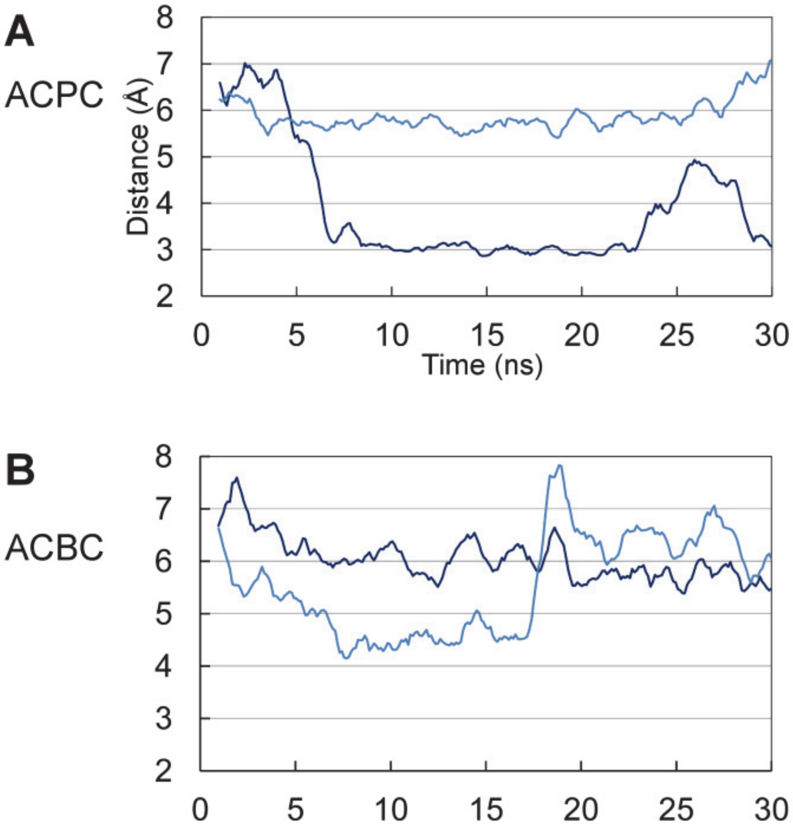

Figure S1. Constraint-free MD simulations of ACPC and ACBC. Free MD simulations starting from open GluN1-LBD are shown for (A) ACPC and (B) ACBC. IHB distance (Gly458^{N}-Gln686^{O}) measurement for two representative repeats is shown for both partial agonists. Simulations with bound ACPC show closure of the LBD (dark blue) and the stable intermediate stage (light blue). In simulations with ACBC, two distinct intermediate stages can be seen: one at 4–5 Å (light blue) and another at 5–6 Å (dark blue, starting from approximately 20 ns).

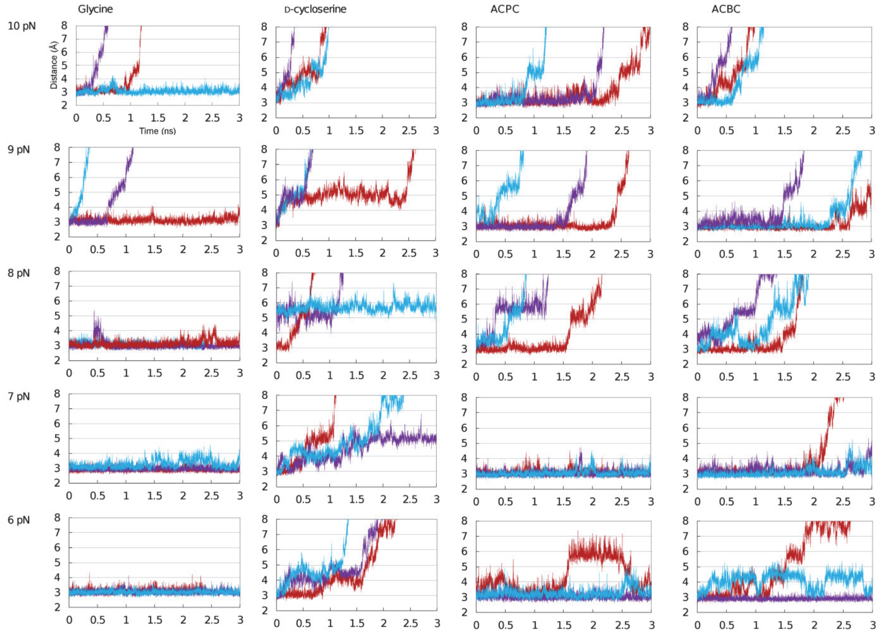

Figure S2. GluN1-LBD opening in SMD simulations. Openings of glycine, D-cycloserine, ACPC and ACBC-bound closed GluN1-LBD in SMD simulations are shown for various external forces. In the simulations, a constant force (6–10 pN) was applied to C^{α} atoms of D2 (Gln536-Ser756) while the C^{α} atoms of D1 (Met394-Tyr535 and Gly757-Ser800) were kept fixed. Three repeats (colored blue, purple and red) are shown for each ligand and force used.

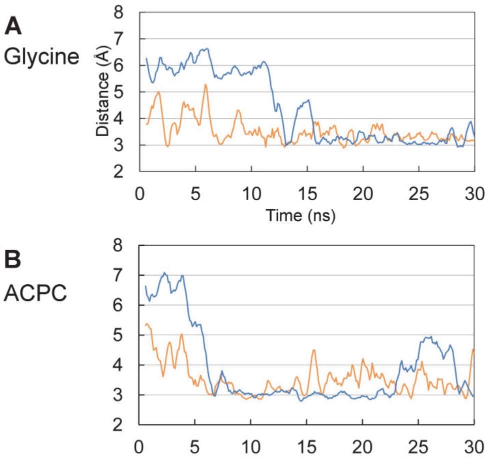

Figure S3. Closure mechanism of glycine and ACPC-bound GluN1-LBD. Distance measurements of Gly458^{N}-Gln686^{O} (blue) and Gln405^{OE1}-Trp731^{NE1} (orange) from (A) glycine and (B) ACPC-bound open-cleft GluN1-LBD are taken from constraint-free MD simulation trajectories. Similar distance measurements for D-cycloserine bound LBD are shown in Figure 4B.

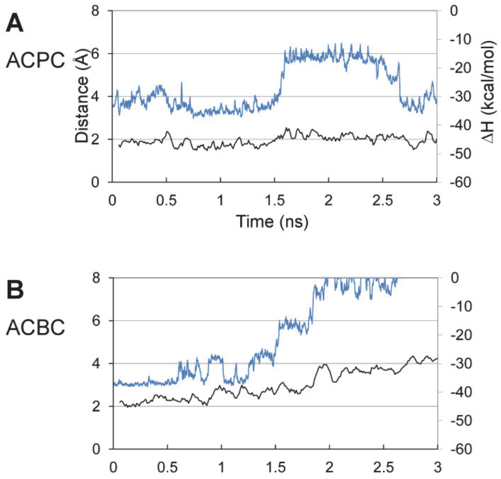

Figure S4. Calculated binding enthalpies (ΔH) from SMD simulations of ACPC and ACBC-bound GluN1-LBD. Compared to D-cycloserine, a similar trend was seen in SMD simulations of (A) ACPC and (B) ACBC: when the LBD opened to an intermediate stage, the ΔH increased only negligibly. With ACPC, this is seen from 1.5 to 2.5 ns and with ACBC, from 1.0 to 1.8 ns. IHB distance is shown in blue and the ΔH, estimated by the MMGB/SA method, in black.

III

MMGBSA AS A TOOL TO UNDERSTAND THE BINDING AFFINITIES OF FILAMIN-PEPTIDE INTERACTIONS

by

Ylilauri, M. & Pentikäinen, O.T. 2013.

Journal of Chemical Information and Modeling 53, 2626–2633

Reprinted with kind permission of American Chemical Society.

IV

MOLECULAR MECHANISM OF T-CELL PROTEIN TYROSINE PHOSPHATASE (TCPTP) ACTIVATION BY MITOXANTRONE

by

Ylilauri, M., Mattila, E., Nurminen, E.M., Käpylä, J., Niinivehmas, S.P., Määttä, J.A., Pentikäinen, U., Ivaska, J. & Pentikäinen, O.T. 2013.

Biochimica et Biophysica Acta 1834, 1988–1997

Reprinted with kind permission of Elsevier.